ทฤษฎีควอนตัมของรอยต่อโจเซฟสันสำหรับใช้เป็นควอนตัมบิต

นายราชศักดิ์ ศักดานุภาพ

วิทยานิพนธ์นี้เป็นส่วนหนึ่งของการศึกษาตามหลักสูตรปริญญาวิทยาศาสตรมหาบัณฑิต
สาขาวิชาฟิสิกส์ ภาควิชาฟิสิกส์
คณะวิทยาศาสตร์ จุฬาลงกรณ์มหาวิทยาลัย
ปีการศึกษา 2548
ISBN 974-53-2410-8

QUANTUM THEORY OF JOSEPHSON JUNCTION FOR A QUANTUM BIT

Mr. Rachsak Sakdanuphab

A Thesis Submitted in Partial Fulfillment of the Requirements
for the Degree of Master of Science Program in Physics

Department of Physics

Faculty of Science

Chulalongkorn University

Academic year 2005

ISBN 974-53-2410-8

Thesis Title	Quantum Theory of Josephson Junction for a Quantum Bit
By	Mr. Rachsak Sakdanuphab
Field of Study	Physics
Thesis Advisor	Sojiphong Chatraphorn, Ph.D.

Accepted by the Faculty of Science, Chulalongkorn University in Partial Fulfillment of the Requirements for the Master's Degree

..... Dean of the Faculty of Science

(Professor Piamsak Menasveta, Ph.D.)

THESIS COMMITTEE

..... Chairman

(Assistant Professor Pisistha Ratanavararak, Ph.D.)

..... Thesis Advisor

(Sojiphong Chatraphorn, Ph.D.)

..... Member

(Chatchai Srinitiwarawong, Ph.D.)

..... Member

(Somchai Kiatgamolchai, Ph.D.)

ราชศักดิ์ ศักดานุภาพ : ทฤษฎีควอนตัมของรอยต่อโจเซฟสันสำหรับใช้เป็นควอนตัมบิต. (QUANTUM THEORY OF JOSEPHSON JUNCTION FOR A QUANTUM BIT) อ. ที่ปรึกษา : ดร. โศจิพงศ์ ฉัตราภรณ์, 59 หน้า. ISBN 974-53-2410-8.

รอยต่อโจเซฟสันเป็นอุปกรณ์ที่คาดหวังว่าจะนำมาใช้เป็นควอนตัมบิตหรือเรียกอีกอย่างหนึ่งว่า คิวบิตในควอนตัมคอมพิวเตอร์ พฤติกรรมทางไฟฟ้าของรอยต่อโจเซฟสันสามารถอธิบายได้ด้วยแบบจำลอง RCSJ ซึ่งจะคล้ายกับการเคลื่อนที่แบบคลาสสิคของอนุภาคในพลังงานศักย์แบบกระดานซักผ้าเอียง (tilted washboard) ในงานนี้เราศึกษาถึงคุณสมบัติทางควอนตัมของรอยต่อโจเซฟสันโดยใช้ทฤษฎีควอนตัมและการประมาณทางควอนตัมในการคำนวณและอธิบายผลที่เกิดขึ้น ซึ่งเราพบว่าพลังงานในบ่อศักย์สามารถที่จะถูกควอนไทซ์และนำไปใช้เป็นคิวบิตสำหรับควอนตัมคอมพิวเตอร์ได้ โดยที่อัตราการทะลุผ่านกำแพงศักย์ของระดับพลังงานหนึ่ง ๆ มีค่าเพิ่มขึ้นแบบเอกซ์โพเนนเชียลเมื่อค่ากระแสที่ไบแอสมีค่าสูงขึ้น โดยสถานะกระตุ้นที่หนึ่งมีอัตราการทะลุผ่านมากกว่าสถานะพื้นอยู่ประมาณ 10^3 เท่า ฟังก์ชั่นคลื่นของสถานะต่าง ๆ ในบ่อศักย์มีลักษณะคล้ายกับฟังก์ชั่นคลื่นของการสั่นแบบฮาร์โมนิกทั้งนี้เนื่องจากรูปร่างของบ่อศักย์มีความคล้ายคลึงกัน ส่วนอัตราการทรานซิชันระหว่างระดับพลังงานอันเนื่องจากการแผ่รังสีของคลื่นแม่เหล็กไฟฟ้ามีค่าขึ้นกับขนาดและความถี่ของกระแสไมโครเวฟที่ใส่เข้าไป โดยคาบของการเปลี่ยนสถานะอยู่ในช่วงนาโนวินาที และช่วงเวลาดีโคฮีเรนส์ในรอยต่อโจเซฟสันสามารถคำนวณได้จากการพิจารณา Rabi's oscillation เมื่อมีสัญญาณรบกวนในกระแสที่ไบแอส เราพบว่าช่วงเวลาดีโคฮีเรนส์ขึ้นอยู่กับขนาดของค่ากระแสรบกวน ซึ่งผลในส่วนนี้สามารถบอกถึงความเป็นไปได้ในการนำรอยต่อโจเซฟสันมาใช้เป็นคิวบิต

ภาควิชา.....ฟิสิกส์.....
สาขาวิชา.....ฟิสิกส์.....
ปีการศึกษา.....2548.....

ลายมือชื่อนิสิต...ราชศักดิ์ ศักดานุภาพ...
ลายมือชื่ออาจารย์ที่ปรึกษา...[illegible]...

4672387423 :MAJOR PHYSICS
KEY WORDS: JOSEPHSON JUNCTION / QUBIT / QUANTUM COMPUTATION

RACHSAK SAKDANUPHAB : QUANTUM THEORY OF JOSEPHSON JUNCTION FOR A QUANTUM BIT. THESIS ADVISOR : SOJIPHONG CHATRAPHORN, PH.D., 59 pp. ISBN 974-53-2410-8.

Josephson junction is a one of the promising devices to be used as a quantum bit or known as qubit in a quantum computer. The dynamics of current-bias Josephson junction can be described by using the Resistively and Capacitively Shunted Junction (RCSJ) model which is analogous to the classical motion of a particle in a tilted washboard potential. In this work, quantum theory and approximation methods are used to calculate and explain quantum properties of the Josepson junction. We found that the energy levels in the washboard potential can be quantum mechanically quantized, and thus used as a qubit in quantum computation. The tunneling rate from the n^{th} energy level exponentially increases with bias current and the first excited state is three orders of magnitude more than the ground state. The wave function of the state in the potential well is relatively similar to the harmonic oscillator wave function because of the shape of the washboard potential. The transition rate between the energy levels due to an electromagnetic radiation depends on the amplitude and the frequency of microwave current. The period of the oscillation is in the order of nanoseconds. Finally the decoherence time in Josephson junction can be observed by considering the Rabi's oscillation in the presence of current noise. The decoherence time depends on the magnitude of the current noise. This result can be used to determine the feasibility of using Josephson junction as a qubit.

Department.....Physics.... Student's signature R. Sakdanuphab

Field of study....Physics.... Advisor's signature S. Chatraphorn

Academic year...2005.....

Acknowledgements

I would like to express my great gratitude to my advisor, Dr. Sojiphong Chatraphorn, for his suggestion and discussion on my work. I also wish to thank to Assistant Professor Pisistha Ratanavararak, Dr. Chatchai Srinitiwarawong and Dr. Somchai Kiatgamolchai for serving as a chairman and the thesis committee, respectively.

This thesis was financially supported by the Development and Promotion of Science and Technology Talents Project (DPST), and I also thank to the Condensed Matter Research Group (CMRG) for the facilities. I would like to thank my friend in the CMRG group for helping me in various ways.

Finally, a deep affectionate gratitude is acknowledged to my family for love, understanding, and encouragements throughout the entire study.

Table of Contents

Chapter

List of Tables

List of Figures

CHAPTER I

INTRODUCTION

Quantum computer are promised to solve certain difficult problems in computer science, such as factoring prime number, searching algorithms and running simulations of quantum mechanical system faster than classical one. Quantum computers use a quantum system instead of a classical system, storing information as well as operating computation under the principle of quantum mechanics. Theory of quantum computation has been developed since the last nineteen century, and today there are many quantum systems such as Nuclear Magnetic Resonance (NMR), Trapped Ion, Optical, Solid State, and Superconducting that are used to build quantum computers[1].

Solid state and superconducting devices have been shown to attract more attentions for quantum computation because they are relatively easy to build and scale up with existing fabrication technologies. Josephson junction is one of the promising devices to be used as a quantum bit (qubit) in a quantum computer[2]. Josephson junction is a superconducting device which consists of two superconductors separated by a thin insulating barrier such as $Nb/AlO_x/Nb$ and $Al/AlO_x/Al$. The quantum behaviors of the Josephson junction appear in macroscopic system because the phase difference of the macroscopic wave function of the two superconductors is a macroscopic variable. The dynamics of a current-biased Josephson junction can be described by using a simple model known as the Resistively and Capacitively Shunted Junction (RCSJ) model, which is analogous to the classical motion of a fictitious particle moving in a tilted washboard potential. This potential is the key to study the quantum properties of the Josephson junction such as energy levels in the potential well, state wave functions, tunneling rates through the barrier, transition rate between the energy levels and the decoherence times of

the states. These results are basic knowledge necessary for the experimental work in quantum computation.

In this work, the quantum mechanical properties of the Josephson junction to be used as a quantum bit in quantum computers are studied. First, the energy levels in the washboard potential which the information states 0 and 1 can be stored in the ground state $|0\rangle$ and the first excited state $|1\rangle$ of the junction, respectively. Second, the tunneling rate in the Josephson junction that the particle can tunnel through the potential barrier. This quantum tunneling effect is a problem in computation because a particle prepared in a state inside the well can leave the system. Third, the state wave functions of the qubit that describe the probability of finding the state and the quantum behaviors. Fourth, the transition rates of the states of qubit when interacting with an electromagnetic radiation. A microwave current is applied as a perturbation to observe the transition between the states. Finally, the decoherence times of the Josephson junction in the presence of current noise can be observed by considering the Rabi's oscillations and determine the feasibility of using Josephson junction as a qubit.

In chapter 2, I will discuss the basic concept of quantum computation involving the history of quantum computation, the theory of computation and the necessary conditions for quantum computation. The basics of Josephson junction is described in chapter 3. I will explain the characteristics of ideal Josephson junction and a useful model for describing the junction. In addition, the classical dynamics of the Josephson junction that describe the electrical property of the junction will be shown. In chapter 4, I will present the approximation methods and the calculation details of finding the quantum properties of the Josephson junction. Finally, chapter 5 is the conclusions of this thesis and suggestions for future work.

CHAPTER II

REVIEW OF QUANTUM COMPUTATION

In this chapter, the basic concepts of quantum computation are reviewed. First, the history and the development of quantum computation will be presented for realizing the limit of classical computer. Second, the differences between classical bits and quantum bits are compared, as well as the potential and the power of quantum computer. Finally, the necessary conditions of a quantum computer known as DiVincenzo's criteria will be described.

2.1 History of Quantum Computation

The history of Quantum Computation started in 1982 by a suggestion of R. P. Feynman[3]. He showed the difficulties of simulating quantum mechanical systems on a classical computer and suggested to build a computational device based on the principle of quantum mechanics for avoiding the problems. The potential of simulation capability is important for finding new phenomena in quantum physics, which lead to create new technologies as challenging for physicists and scientists.

In 1964, Gordon Moore, who is now a chairman emeritus of Intel, Corp., proposed the restriction of feature size of transistor on an area of a silicon chip, known as "Moore's law": the numbers of transistor doubly increase every eighteen months[4]. Therefore the feature size decreases continuously as shown in Fig. 2.1. He predicts that the end of the classical device (CMOS) is around year 2015 and leads to the new quantum age. Quantum devices based on quantum mechanics

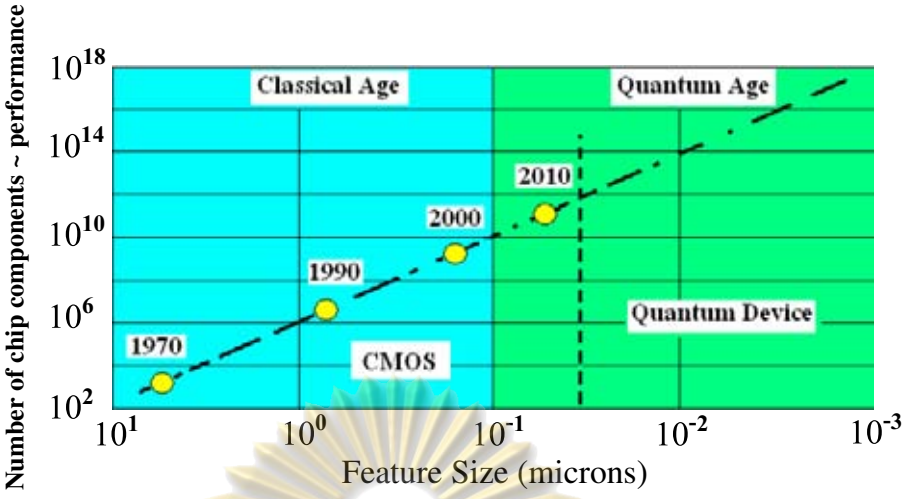

Figure 2.1: The number of chip components in the past to the future[4].

will take place instead of the classical devices. Scientists realize this problem, so they must find new computational devices to replace the classical one.

In 1994, Peter Shor, AT&T's Bell Labs scientist, proposed a quantum algorithm known as "Shor's algorithm" for factoring prime numbers, running in $O((\log N)^3)$ steps[5], where N is a factoring number. Comparing with classical algorithm, the well known factoring algorithm runs in $O(\exp[(64/9)^{1/3}(\ln N)^{1/3}(\ln \ln N)^{2/3}])$ steps which is an exponential problem on the classical computer, depending on the digit number of N. This problem cannot be solved for a large number. For example, N is a 129 digit number, the entire factorization with this algorithm takes about eight months in computing on 1600 workstations around the world (RSA129)[6]. If N is increased to 250 digit number, the factorization will take about 800,000 years with the same computing power. This problem is almost impossible to solve on the classical computer. On the contrary, the quantum computational device can reduce the running steps to a polynomial problem that can be solved in relatively much shorter time.

There is also another advantage of quantum computer over classical one such as the security problem. Today, the information is very important and valuable. The public-key cryptography is necessary for the information security. The components of the cryptography are the information and a secret code. A sender encrypts the information with the secret code and send to the public. A receiver, who has

a specific key, decrypts the public message and then obtains the true information. It has been concerned that the public-key cryptography will be breakdown in the future if a quantum computer is successfully realized.

2.2 Classical Bit and Quantum Bit

In the classical computation, the information are represented by the binary digit (bit) either 0 or 1, and use the classical systems such as ON state and OFF state of a switch, or the classical voltage levels representing the state of a classical bit as shown in Fig. 2.2. For multiple bits, the state of N bits can be written by 2^N integer value, 00...0, 00...1, ..., and 11...1. For example, the state of 5 bits may be written as 10110 and can be represented by the voltage signal as shown in Fig. 2.3. The states of classical bits will be operated by Boolean logic gates such as AND gate, OR gate and XOR gate etc., which have specific characteristics. The integrated circuits that consist of a set of Boolean logic gates are used to compute the information.

In the quantum computation, the basic concepts are based on the classical computation but under the laws of quantum mechanics. Quantum computation uses a quantum system instead of the classical system to store information and perform computing. The information states 0 and 1 can be stored in the quantum state of a quantum system, which can be considered as for example a two-level system such as a system of ground state and first excited state of an atom or a

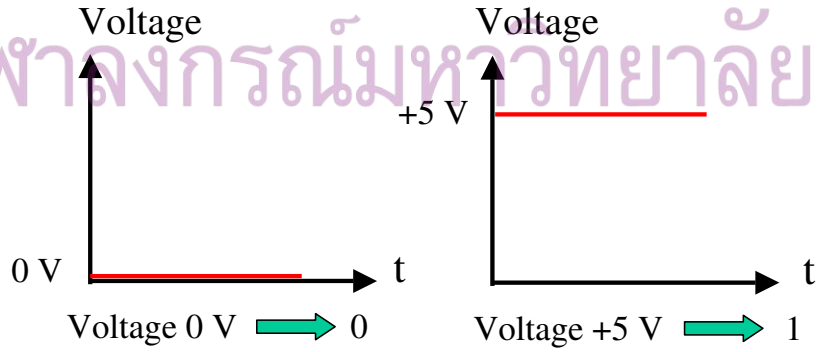

Figure 2.2: The voltage level for representing a classical bit.

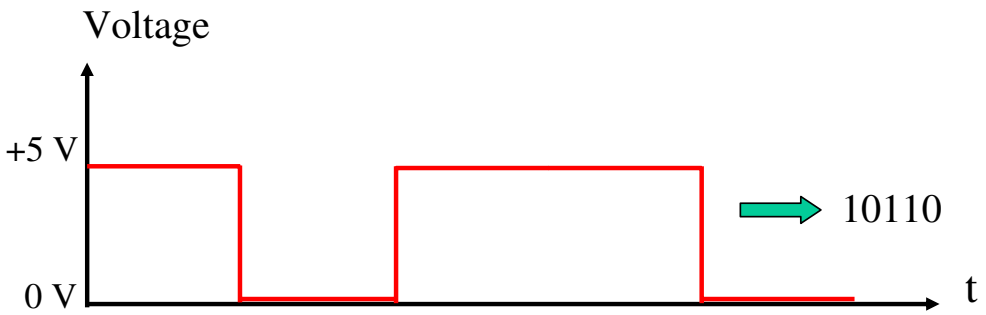

Figure 2.3: The voltage signal for representing a state of 5 bits.

system of spin up and spin down of an electron as shown in Fig. 2.4 and Fig. 2.5, respectively. Usually, the lower state is represented by a qubit $|0\rangle$ and the higher state is represented by a qubit $|1\rangle$. In general, state of a qubit $|\Psi\rangle$ can be a superposition of basis states $|0\rangle$ and $|1\rangle$, given by

$$|\Psi\rangle = \alpha|0\rangle + \beta|1\rangle, \tag{2.1}$$

where α and β are complex numbers representing a probability amplitude of a system being found in $|0\rangle$ state and $|1\rangle$ state, respectively, and thus $|\alpha|^2+|\beta|^2 = 1$. Considering a state of multiple qubits, e.g. the state of two qubits can be written in the superposition of four basis states as

$$|\Psi\rangle = a|00\rangle + b|01\rangle + c|10\rangle + d|11\rangle, \tag{2.2}$$

where $|a|^2 + |b|^2 + |c|^2 + |d|^2 = 1$. In general, the state of N qubits is the superposition of 2^N basis states represented by

$$|\Psi\rangle = \sum_{00\ldots0}^{11\ldots1} c_x|x\rangle, \tag{2.3}$$

and $\sum |c_x|^2 = 1$ or represented by a vector in 2^N dimensions (Hilbert space) as shown in Fig. 2.6. For the quantum computation, the state of qubits is operated by quantum gates such as Pauli gate, Hadamard gate, and Controlled-Not gate etc[7]. The integrated of the quantum gates called quantum circuits are used for computing on quantum computer. The superposition principle permits all basis states of qubits to be operated simultaneously. Thus there are a large number of computations at a time. For an example, if a state of N qubits is operated by a quantum gate, the 2^N basis states of qubits are performed at the same time.

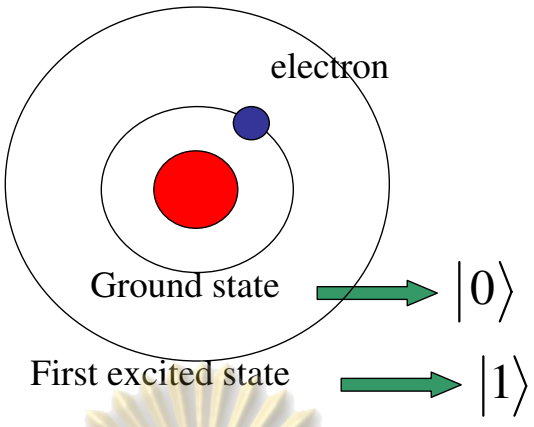

Figure 2.4: The ground state and the first excited state of atom for representing qubit.

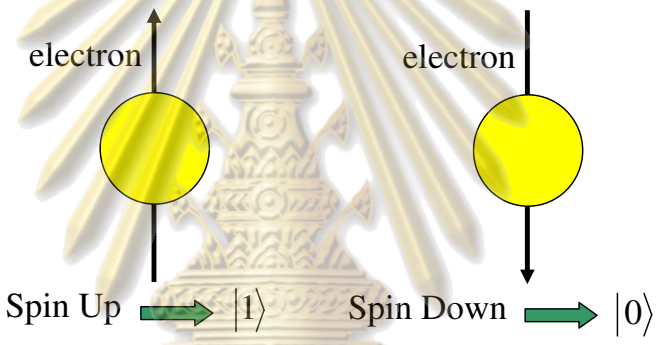

Figure 2.5: The spin up and spin down of an electron for representing qubit.

Hence, quantum computer is more powerful equipment than any existing or the future classical computer[7].

2.3 DiVincenzo's criteria

DiVincenzo's criteria is the necessary conditions of quantum computation that involve the capability for using a quantum system to build a quantum computer. The quantum system will be a good candidate, if it fulfils the five criteria[1]:

1. A scalable physical system of well-characterized qubits.

2. The ability to initialize the state of the qubits to a simple fiducial state.

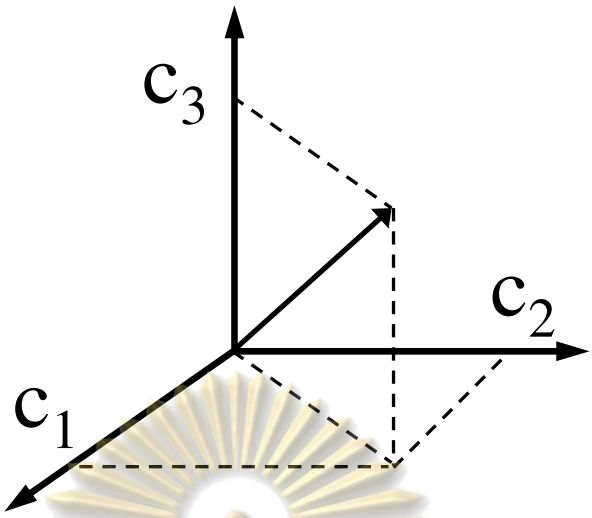

Figure 2.6: The 2^N dimension of Hilbert space.

3. Long (relative) decoherence times, much longer than the gate-operation time.

4. A universal set of quantum gate.

5. A qubit-specific measurement capability.

And the two additional criteria, which are necessary conditions for quantum computer networkability are:

1. The ability to interconvert stationary and flying qubits, and

2. The ability to faithfully transmit flying qubits between specified locations.

Today, there are many quantum systems such as NMR, Trapped Ion, Optical, Solid State, and Superconducting devices, proposed to build quantum computers[7]. The nuclear magnetic resonance (NMR) is the first physical system to be used for building a quantum computer. A qubit is represented by the spins of an atomic nucleus. The state $|0\rangle$ and $|1\rangle$ can be initialized by polarizing the spins in a strong magnetic field. The quantum operations or quantum gates are constructed from magnetic field pulses applied to the spins. The precessing magnetic moment induces a voltage signal for reading out the state of qubit. The drawback of this system is that it cannot scale up in the number of qubits because the effective

pure state preparation schemes reduce the signal exponentially with the number of qubits and the NMR implementation is too large.

The ion trap quantum computer use hyperfine (nuclear spin) state of an atom and the lowest level vibration modes (phonon) of trapped atoms to represent qubits. The initial state can be prepared by cooling the atom into their motional ground state, and hyperfine ground state (by trapping and using optical pumping). The quantum gates are constructed from the application of laser pluses for manipulating the atomic states and the state of qubit can be readout by measuring the population of hyperfine states. The drawback of ion trap is that the phonon lifetimes are short and the ions are difficult to prepare in their motional ground states.

The optical photon quantum computer uses the location of single photon between two modes, $|01\rangle$ and $|10\rangle$, or polarization to represent qubit. The initial state can be prepared by creating single photon states (by attenuating laser light). The quantum gates are constructed from phase shifters, beamsplitters, and nonlinear Kerr media, which allow two single photons to cross phase modulation. The single photon can be detected by using a photomultiplier tube for reading out the state of qubit. The drawback of the optical photon is that the absorption loss of the nonlinear Kerr media with large ratio of cross phase modulation strength is difficult to realize.

The solid state based quantum dot quantum computer uses the spin of a single electron confined in a quantum dot to represent qubit. The quantum dot can be defined by 50-nm-wide electrostatic gates on top of a AlGaAs/GaAs two-dimensional electron gas (2-DEG), or by three-dimensional (3-D) confinement in a patterned semiconductor heterostructure. The initial state is in the ground state spin-up, prepared by place in the equilibrium at 300 mK and 5 tesla. The quantum gates are constructed from an all-electrical control of spin via electrical gates. The charge and coulomb interactions of the electrons allow fast gate operation and readout the state of qubit.

The superconducting qubit is made with the Josephson junctions that the information can be stored in either the charge on a nanoscale superconducting island, the flux or phase drop in a circulating current, or in the energy levels in a

single junction. The initial state can be prepared by cooling the qubit to extremely low temperature about millikelvin (mK). The quantum gates are constructed by using pulses of microwave radiation to perform qubit operations. The state of the qubit can be read out by measuring the switching current in phase qubit or by measuring the inductance in flux qubit. The inherently low dissipation of superconductors make possible long coherence times, and integrated circuit technology allows scaling to large and complex circuits.

The solid state and the superconducting systems are available on the DiVincenzo's criteria because they will be relatively easy to build and scale up with existing fabrication technology. The initializing the state can be prepared by cooling the system, and a decoherence time is long enough. In this work, I am interested in the superconducting system using the energy levels in a single Josephson junction as a candidate for qubit. I will study the classical characteristics and quantum properties of Josephson junction for using the junction as a quantum bit in quantum computer.

2.4 Summary

In this chapter, the basic concepts of quantum computation have been briefly discussed. The problems of simulating quantum systems and the restriction of feature size of transistor lead to the end of classical computer. The theory of quantum computation are based on the classical computation under the laws of quantum mechanics. The basic unit of quantum computation is a quantum bit that can be represented by a quantum system. There are many quantum systems proposed to build quantum computers. Josephson junction is a one of the promising devices to be used as a quantum bit in a quantum computer. Josephson junction is also on the DiVincenzo's criteria and has the quantum behaviors appeared in macroscopic system. The theoretical background of Josephson junction will be discussed in the next chapter.

CHAPTER III

THEORETICAL BACKGROUND OF JOSEPHSON JUNCTION

In this chapter, the theoretical background of Josephson junction is described. First, the characteristics of Josepson junction that involve the structure and the properties will be explained. Second, a simple model that describes the dynamics of the Josephson junction is used to find the classical equation of motion and the potential energy of the system. Finally, I will show how to obtain the solution for equation of motion and describe the electrical property of the junction.

3.1 The characteristics of Josephson junction

A superconductor was discovered in 1911 by Heike Kamerlingh-Onnes who showed that, below a critical temperature, a superconductor can conduct electricity without electrical resistance. He found that a high magnetic field could destroy the superconductivity. Then, in 1933, W. Meissner and R. Ochsenfeld discovered the ideal diamagnetism of a superconductor. In the presence of an applied magnetic field, a superconductor can expel the magnetic field from the interior, thus the field inside becomes zero. The superconductivity was not well understood on the theoretical basis until 1975. John Bardeen, Leon Cooper and Robert Schrieffer published the BCS theory for explaining the properties of superconductor in the microscopic scale[8]. In superconductor, two electrons bind together to form a

Cooper pair. The attractive interaction between the electrons involves the interaction between the electrons and the vibrating crystal lattice (phonons). When an electron moves through a conductor, it will cause an increasing of the positive charges concentration in the lattice around it, however the net charge is still the same. This can attract another electron with momentum opposite to the first for holding together. A Cooper pair has a certain binding energy that is higher than the energy provided by collisions from oscillating atoms in the conductor. The electron pair will stick together and resists all collisions, thus not experiencing a resistance. An electron has a spin of 1/2 and thus the total spin of the Cooper pair can be either $S = 0$ (singlet state) or $S = 1$ (triplet state). The wave function of the Cooper pair is the product of the orbital and spin parts that is asymmetric under the interchange of the pair. Therefore, the orbital angular momentum of the wave function for a spin-singlet is symmetric that is $L = 0$ (s-wave) and $L = 2$ (d-wave), and that for a spin-triplet is asymmetric $L = 1$ (p-wave). The conventional Cooper pair has the total spin of zero with the s-wave pairing. The Cooper pair acts as a boson that can occupy the same quantum state. These bosons show the Bose-Einstein condensation in which the states of Cooper pair form a coherent matter. This refers to a macroscopic wave function that is the key property of superconducting state.

The discovery of high-temperature superconductors lead to many applications of superconductor that have been used in various fields. For example, magnetic-levitation can be used in transport vehicles. In Japan, the Yamanashi MLX01 MagLev train can be made to float on the strong superconducting magnets for eliminating the frictions between the train and its tracks. Although the speed of the train is incredible at speed of 361 mph (581 kph), the strong magnetic fields can create a bio-hazard to human. In medicine, Magnetic Resonance Imaging (MRI) is used to create images of opaque organ in living organisms by impinging a strong superconductor-derived magnetic field into the body. The hydrogen atom in the human body such as water and fat molecules are forced to accept energy from the magnetic field. Then, they release the energy with a resonance frequency that can be detected and converted graphically by a computer. The MRI is a useful mechanism for saving human life. A very sensitive measurement of magnetic fields

can be made with the Superconducting Quantum Interference Devices (SQUIDs), which can detect the changes of magnetic flux in order of less than $10^{-14}Wb$. These devices have applications in medicine, geology and other fields. However, the BCS theory is not well suited for explaining high-temperature superconductor because it cannot describe some aspects of the high-temperature superconductor such as its high critical temperature, the small change of the critical temperature with the implantation of paramagnetic impurities, etc.

Josephson junction is a superconducting device, which consists of two superconductors separated by a thin insulating barrier such as $Nb/AlO_x/Nb$ and $Al/AlO_x/Al$ as shown in Fig. 3.1. The two structures are made of conventional superconductor. One can also build Josephson junction from high-temperature superconductor. Considering the structure of Josephson junction, the Cooper pair can pass through a thin insulating barrier because of quantum mechanical effect called "tunneling effect". The tunneling current in the junction was predicted by Brian D. Josephson[9] who received the Nobel prize in 1973. The two separated superconductors can be described by two wave functions Ψ_1 and Ψ_2. The time-dependent Schrödinger equations of the two systems are

$$\frac{\partial \Psi_1}{\partial t} = \frac{-iE_1\Psi_1}{\hbar}, \tag{3.1}$$

$$\frac{\partial \Psi_2}{\partial t} = \frac{-iE_2\Psi_2}{\hbar}. \tag{3.2}$$

However, there is a weak coupling between the systems due to the exchange of the Cooper pairs between the superconductors[10]. Hence the coupling terms K may

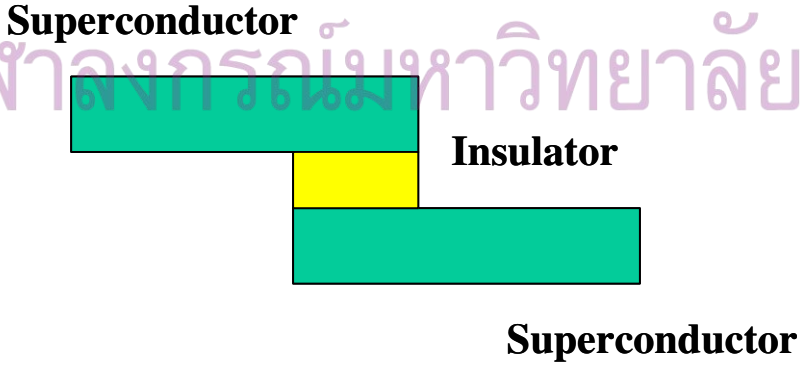

Figure 3.1: The structure of Josephson junction.

be added into Eq.(3.1) and Eq.(3.2)

$$\frac{\partial \Psi_1}{\partial t} = \frac{-i}{\hbar}(E_1\Psi_1 + K\Psi_2), \tag{3.3}$$
$$\frac{\partial \Psi_2}{\partial t} = \frac{-i}{\hbar}(E_2\Psi_2 + K\Psi_1). \tag{3.4}$$

In the condensation of the electrons pairs, the states of the Cooper pairs occupy the same ground state and form a coherent matter wave that refers to a macroscopic wave function. The wave function of the macroscopic two states system can be written in terms of particle density n_s and phase of the wave function ϕ as

$$\Psi_1 = \sqrt{n_{s1}}e^{i\phi_1}, \tag{3.5}$$
$$\Psi_2 = \sqrt{n_{s2}}e^{i\phi_2}, \tag{3.6}$$

corresponding to the superconductor 1 and 2, respectively. Inserting Ψ_1 and Ψ_2 into the Eq.(3.3) and Eq.(3.4), one obtains

$$\frac{\dot{n}_{s1}}{2\sqrt{n_{s1}}}e^{i\phi_1} + i\sqrt{n_{s1}}e^{i\phi_1}\dot{\phi}_1 = \frac{-i}{\hbar}(E_1\sqrt{n_{s1}}e^{i\phi_1} + K\sqrt{n_{s2}}e^{i\phi_2}), \tag{3.7}$$
$$\frac{\dot{n}_{s2}}{2\sqrt{n_{s2}}}e^{i\phi_2} + i\sqrt{n_{s2}}e^{i\phi_2}\dot{\phi}_2 = \frac{-i}{\hbar}(E_2\sqrt{n_{s2}}e^{i\phi_2} + K\sqrt{n_{s1}}e^{i\phi_1}). \tag{3.8}$$

By comparing the real and the imaginary parts from both sides of Eq.(3.7) and Eq.(3.8), the relations are found

$$\frac{1}{2}\frac{\dot{n}_{s1}}{\sqrt{n_{s1}}} = \frac{K}{\hbar}\sqrt{n_{s2}}\sin(\phi_2 - \phi_1), \tag{3.9}$$
$$\frac{1}{2}\frac{\dot{n}_{s2}}{\sqrt{n_{s2}}} = \frac{K}{\hbar}\sqrt{n_{s1}}\sin(\phi_1 - \phi_2), \tag{3.10}$$
$$i\sqrt{n_{s1}}\dot{\phi}_1 = \frac{-i}{\hbar}(E_1\sqrt{n_{s1}} + K\sqrt{n_{s2}}\cos(\phi_2 - \phi_1)), \tag{3.11}$$
$$i\sqrt{n_{s2}}\dot{\phi}_2 = \frac{-i}{\hbar}(E_2\sqrt{n_{s2}} + K\sqrt{n_{s1}}\cos(\phi_1 - \phi_2)). \tag{3.12}$$

Following the conditions that the exchange rate of the Cooper pairs between superconductor 1 and 2 must be equal, therefore $n_{s1} = -n_{s2}$ and the two superconductors are identical $n_{s1} = n_{s2}$. According to Eq.(3.9) and Eq.(3.10), one obtains

$$\dot{n}_{s1} = \frac{2K}{\hbar}n_{s1}\sin(\phi_2 - \phi_1) = -\dot{n}_{s2}. \tag{3.13}$$

If one multiplies the particle density with the volume of superconductor V_p that yields the change of the particle numbers, and the charge of the Cooper pair $2e$, the electric current I_s called the "supercurrent" is got

$$I_s = I_c\sin(\phi_2 - \phi_1), \tag{3.14}$$

where $I_c = 4KeV_p n_s/\hbar$ is the critical current of the junction. This is the first Josephson relation or known as the dc Josephson relation. The supercurrent depends on the critical current and the phase different across the two superconductors. From Eq.(3.11) and Eq.(3.12), one found

$$\frac{d}{dt}(\phi_1 - \phi_2) = \frac{2eV}{\hbar}, \tag{3.15}$$

where $E_2 - E_1 = 2eV$ and V is a finite voltage across junction. This is the second Josephson relation or known as the ac Josephson relation in case of no magnetic fields. The voltage depends on the time derivative of the phase difference. If the voltage across junction is applied, the phase difference will increase linearly with time

$$\phi_1 - \phi_2 = \frac{2\pi}{\Phi_0} Vt + \phi(t = 0). \tag{3.16}$$

Note that $\Phi_0 = h/2e$ $(2.07 \times 10^{-15} Wb)$ is the flux quantum. In general, if magnetic field is applied to the Josepson junction described by a vector potential $\vec{A}$ $(\vec{\nabla} \times \vec{A} = \vec{B})$, and by using the theory of symmetry and invariance principle, the phase difference can be replaced by the gauge-invariance phase difference across the junction defined by[11]

$$\gamma = \phi_2 - \phi_1 - \frac{2\pi}{\Phi_0} \int_1^2 \vec{A} \cdot d\vec{l}. \tag{3.17}$$

Hence, the first Josephson relation can be rewritten as

$$I_s = I_c \sin(\gamma), \tag{3.18}$$

and the second Josepson relation becomes

$$V = \frac{\hbar}{2e} \frac{d\gamma}{dt}. \tag{3.19}$$

3.2 RCSJ model

The Josephson junction can be considered by using the equivalent circuit diagram known as the RCSJ (Resistively and Capacitively Shunted Junction) model as shown in Fig. 3.2. This model was proposed by W.C. Stewart and D.E. McCumber [12, 13]. Because the geometry of Josephson junction is similar to a parallel plate

capacitor, it has a finite capacitance C. The real junction has a shunted resistance R due to a finite voltage across the junction. The magnitude of the resistance depends on the type of junction such as S-c-S junction, S-N-S junction and S-I-S junction where S, I, N and c are superconductor, insulator, normal metal, and constriction, respectively as seen in Fig. 3.3. J.J. is a circuit symbol of the Joephson junction described by the Josephson relation. By using the Kirchhoff's current law, the total bias current I_{dc} through the junction can be written as

$$I_{dc} = C\frac{dV}{dt} + \frac{V}{R} + I_c \sin\gamma. \tag{3.20}$$

Note that, a current noise is neglected from the junction. The first term on the right hand side is the displacement current across the capacitor. The second term is the current through the resistance and the last term is the supercurrent through the junction. Inserting the second Josephson relation into Eq.(3.20), one obtains

$$I_{dc} = C[\frac{\hbar}{2e}]\frac{d^2\gamma}{dt^2} + \frac{1}{R}[\frac{\hbar}{2e}]\frac{d\gamma}{dt} + I_c \sin\gamma. \tag{3.21}$$

This is a non-linear second order differential equation. The numerical solution of the differential equation will be discussed in next section. Multiplying Eq.(3.21) with $\hbar/2e$, one obtains

$$C[\frac{\hbar}{2e}]^2\frac{d^2\gamma}{dt^2} + \frac{1}{R}[\frac{\hbar}{2e}]^2\frac{d\gamma}{dt} + \frac{d}{d\gamma}(-\frac{\hbar}{2e}(I_c\cos\gamma + I_{dc}\gamma)) = 0. \tag{3.22}$$

By comparing Eq.(3.22) with the classical equation of motion

$$m\frac{d^2x}{dt^2} + 2\eta\frac{dx}{dt} + \frac{dU}{dx} = F(t), \tag{3.23}$$

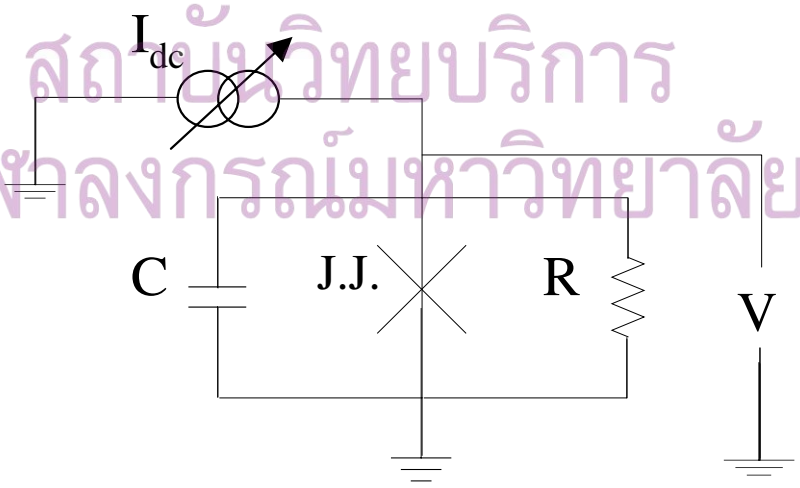

Figure 3.2: The equivalent circuit diagram of Josephson junction.

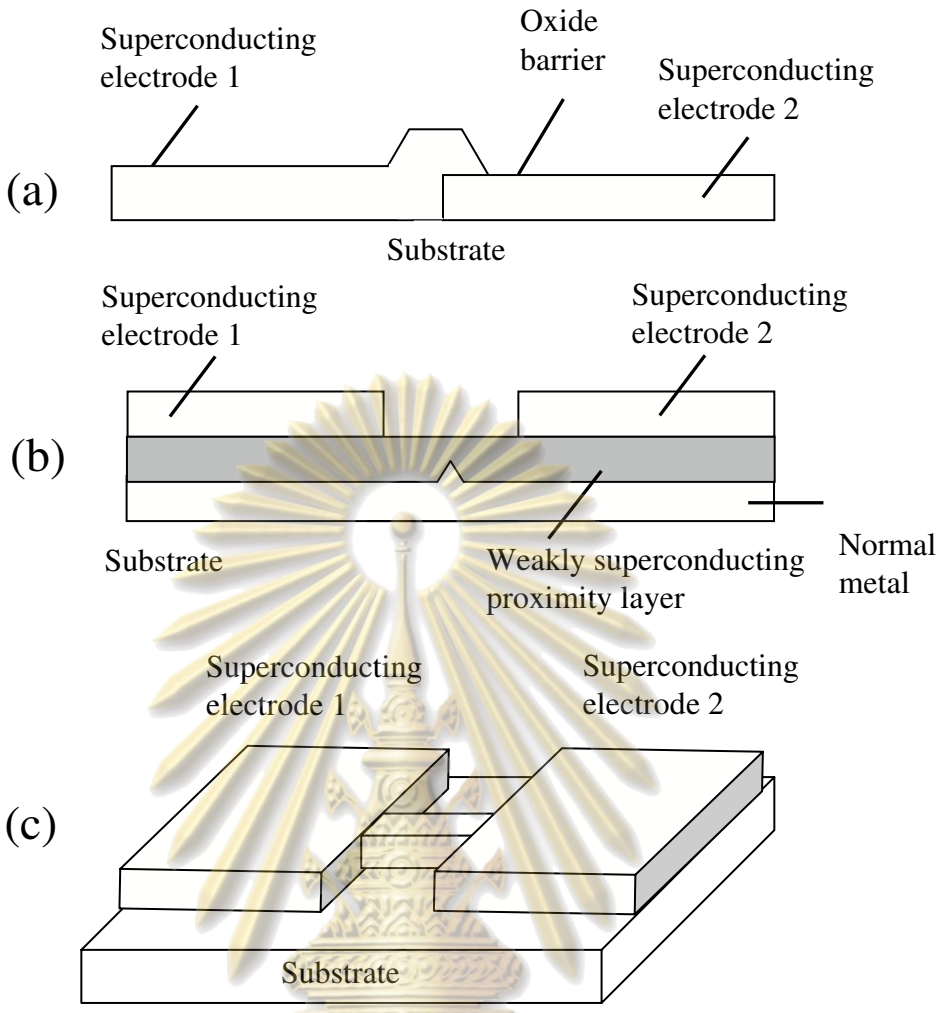

Figure 3.3: The several type of Josephson junction (a) S-I-S (b) S-N-S and (c) S-c-S.

one can see that γ is the dynamical variable in the Josephson junction, $C[\frac{\hbar}{2e}]^2$ is equivalent to a mass m, $\frac{1}{R}[\frac{\hbar}{2e}]^2$ is corresponding to the dragging term and

$$U(\gamma) = -\frac{\hbar}{2e} I_c(\cos\gamma + \frac{I_{dc}}{I_c}\gamma) \tag{3.24}$$

is the potential energy of the system. This potential is known as the tilted wash-board potential as seen in Fig. 3.4. The tilt of the potential depends upon the applied current I_{dc}. This potential will be used to find the energy quantization and study other quantum behaviors of the Josephson junction such as tunneling rates, wave functions, transition rates, and decoherence times in the next chapter.

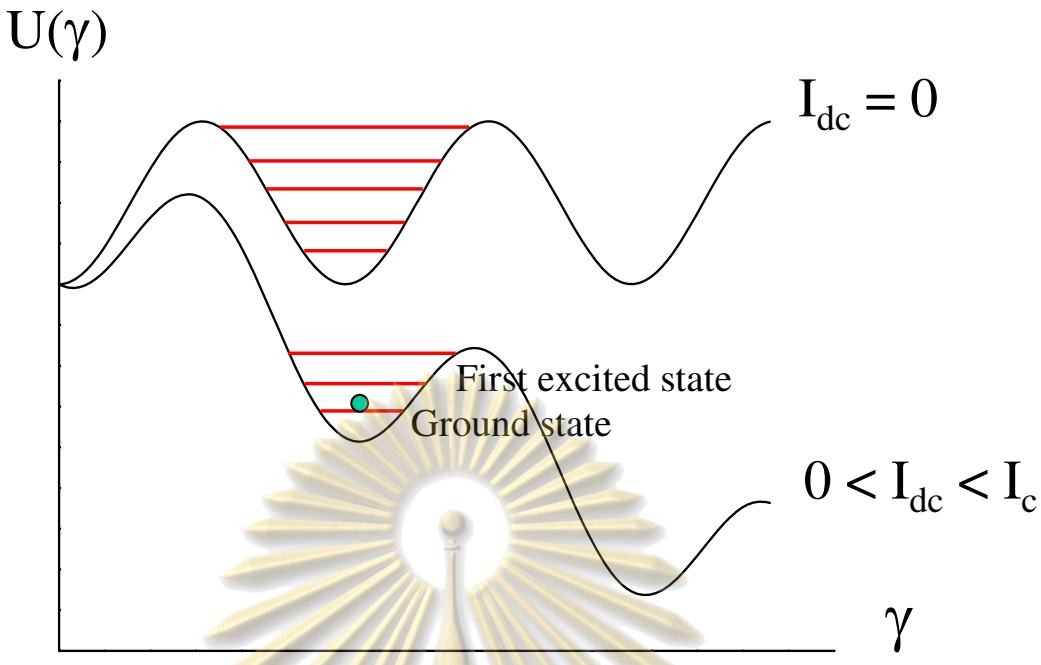

Figure 3.4: The tilted washboard potential.

3.3 Classical dynamics of Josephson junction

In this section, the solution to the equation of motion will be found and describe the electrical property of the Josephson junction. Since Eq.(3.21) cannot be solved analytically, I use a numerical method to solve the equation of motion. From the equation of motion

$$C[\frac{\hbar}{2e}]\frac{d^2\gamma}{dt^2} + \frac{1}{R}[\frac{\hbar}{2e}]\frac{d\gamma}{dt} + I_c \sin\gamma = I_{dc}, \tag{3.25}$$

I introduce a dimensionless variable $\tau = (2eI_cRt)/\hbar$ called "dimensionless time" and substitute with time t. The second order differential equation is obtained

$$\beta\frac{d^2\gamma}{d\tau^2} + \frac{d\gamma}{d\tau} + \sin\gamma = \frac{I_{dc}}{I_c}, \tag{3.26}$$

where $\beta = (2eI_cR^2C)/\hbar$ is called a damping parameter. There are two important parameters β and I_{dc}/I_c. The parameter β depends on the junction design and the other parameter is the ratio of the applied bias current and the critical current. The value of the parameters and the initial condition $\gamma(t = 0)$ and $\dot{\gamma}(t = 0)$ are set before solving the differential equation. Note that, the dot is now the derivative with respect to the dimensionless time. By using the approximation of

the derivative defined by

$$\dot{\gamma}(\Delta\tau) = \ddot{\gamma}(0)\Delta\tau + \dot{\gamma}(0), \tag{3.27}$$

$$\gamma(\Delta\tau) = \dot{\gamma}(0)\Delta\tau + \gamma(0), \tag{3.28}$$

this approximation can be applied to the differential equation. When the bias current is below the critical current, the phase difference is a constant as shown in Fig. 3.5 thus the voltage across the junction is zero by the second Josephson relation. When the bias current is more than the critical current of the junction, the phase difference increases and oscillates in time, thus a finite voltage across the junction occurs, as shown in Fig. 3.6. The average voltage V can be calculated from the solution of dimensionless time derivative of the phase difference as shown in Fig. 3.7 using the relation

$$\dot{\gamma}_{av} = \frac{1}{T}\int_0^T \dot{\gamma}(\tau)d\tau = \frac{V_{av}}{I_c R}. \tag{3.29}$$

The electrical property of the junction can be described by I-V characteristic that depends on the parameters β and I_{dc}/I_c. Figure 3.8 is an I-V characteristic of the junction for a small damping parameter ($\beta = 0.1$). There is an average voltage when the bias current is more than the critical current. In the other case, for a damping parameter $\beta > 1$, there are two stable solutions of the differential equation in some region where $I_{dc} < I_c$. One solution is the normal solution $V = 0$ (for the initial condition $\dot{\gamma}(0) = 0$ and $\gamma(0) = 0$) as shown in Fig. 3.9. The second solution is that there is an average voltage (for the initial condition $\dot{\gamma}(0) = constant$ and $\gamma(0) = constant$) as shown in Fig. 3.10. Therefore, the I-V characteristic becomes hysteretic as shown in Fig. 3.11 when $\beta > 1$. The hysteretic curve of I-V characteristic can be explained by considering a model of a massive particle sliding down the tilted washboard potential as shown in Fig. 3.12. When $I_{dc} = 0$, one can see that the particle stays at a minimum of the potential well. If the bias current I_{dc} is raised, the well becomes shallow but the particle still stays in the well. When the bias current is more than the critical current, the particle can roll down the washboard potential, resulting in the change of the phase difference i.e. a finite voltage across the junction occurs. When the bias current is decreased below the critical current, the massive particle is still under motion due to the inertia of the particle (mass). The inertia depends on the value

of damping parameter β. The particle return trapped in the well when the bias current reach a retrapping current (I_R) where the effect of inertia is less than the effect of damping. The voltage across the junction becomes zero.

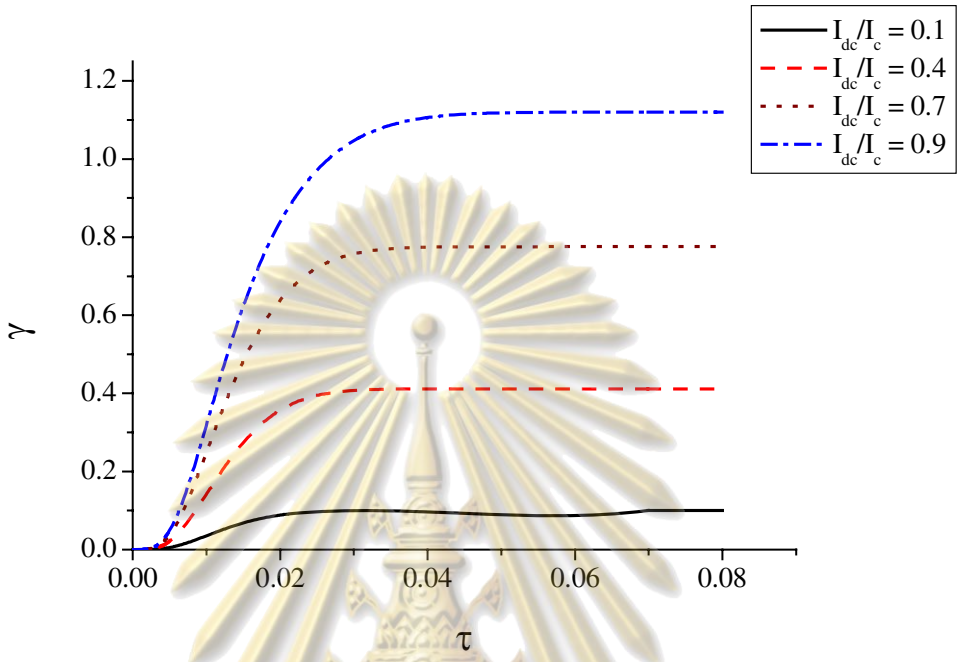

Figure 3.5: The solution of γ when $I_{dc} < I_c$.

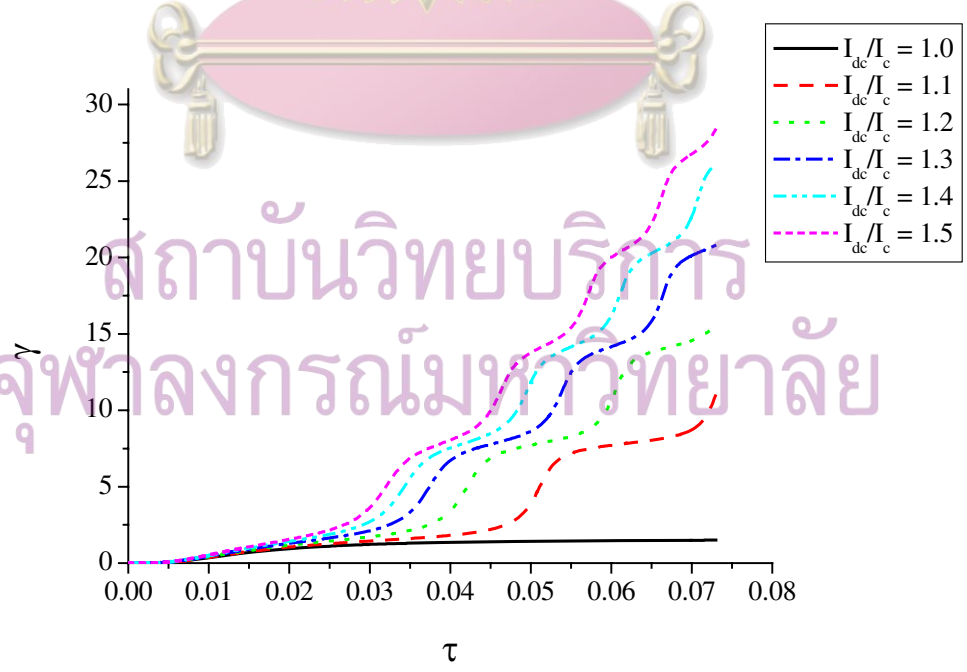

Figure 3.6: The solution of γ when $I_{dc} > I_c$.

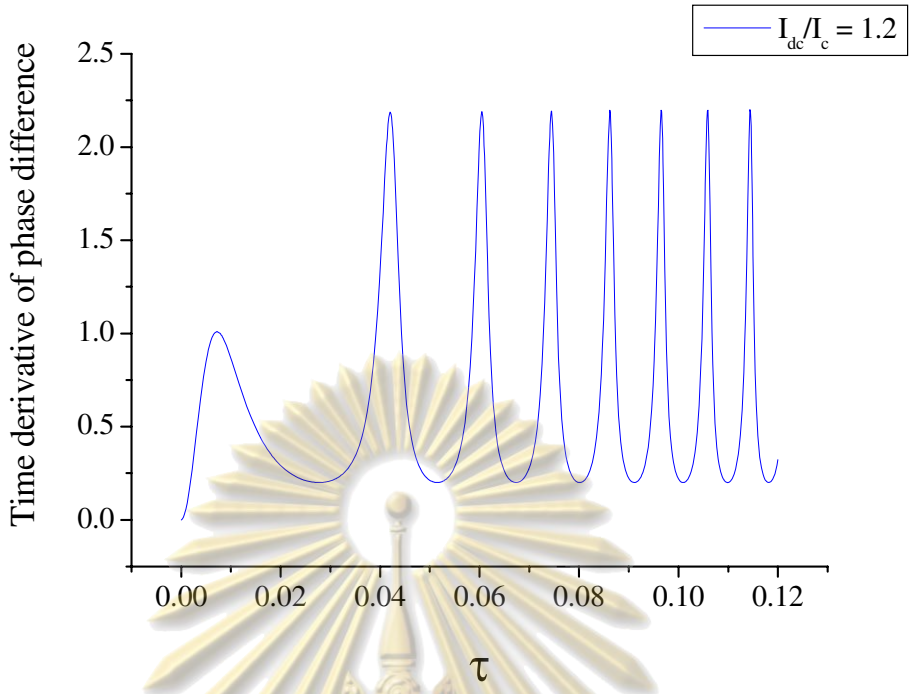

Figure 3.7: The solution of $\dot{\gamma}$ when $I_{dc} = 1.2$.

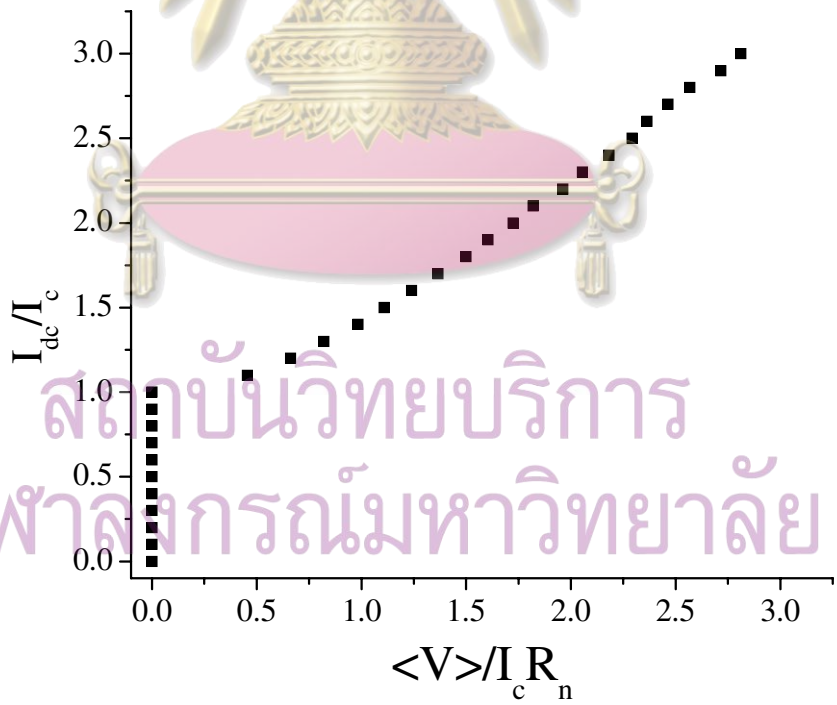

Figure 3.8: The current-voltage characteristic of Josephson junction with $\beta = 0.1$.

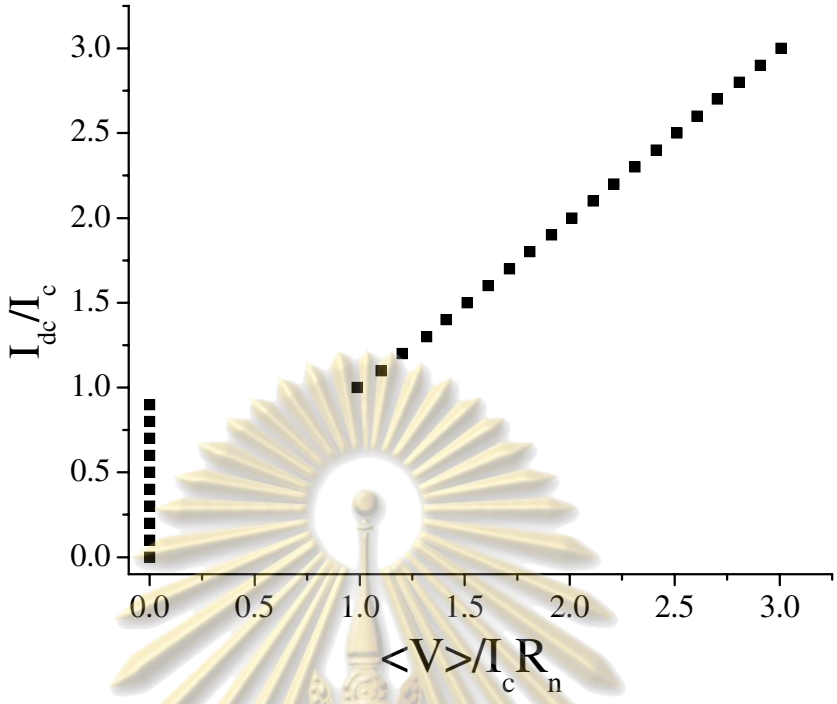

Figure 3.9: The first solution of I-V characteristic with $\beta = 4$.

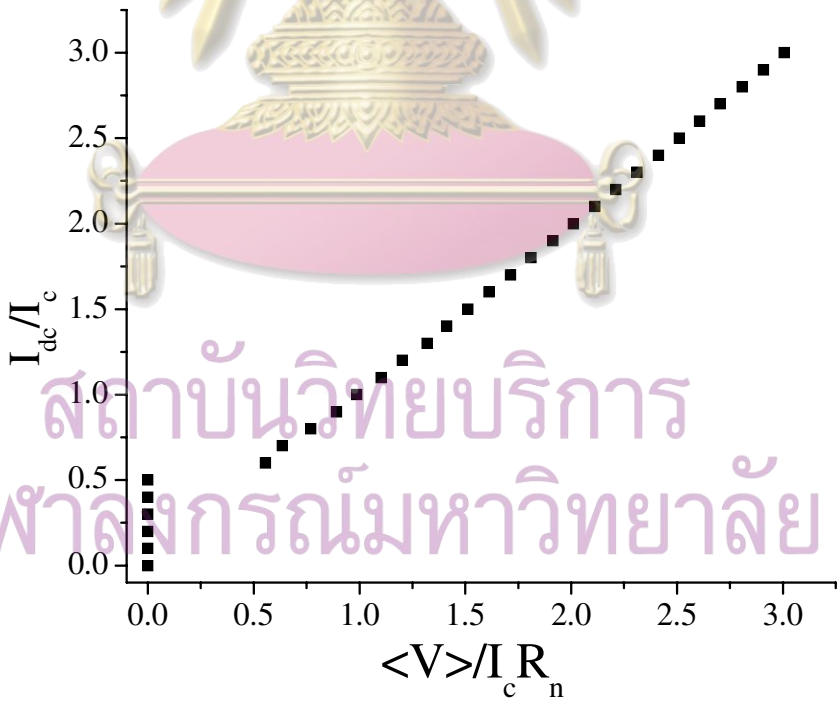

Figure 3.10: The second solution of I-V characteristic with $\beta = 4$.

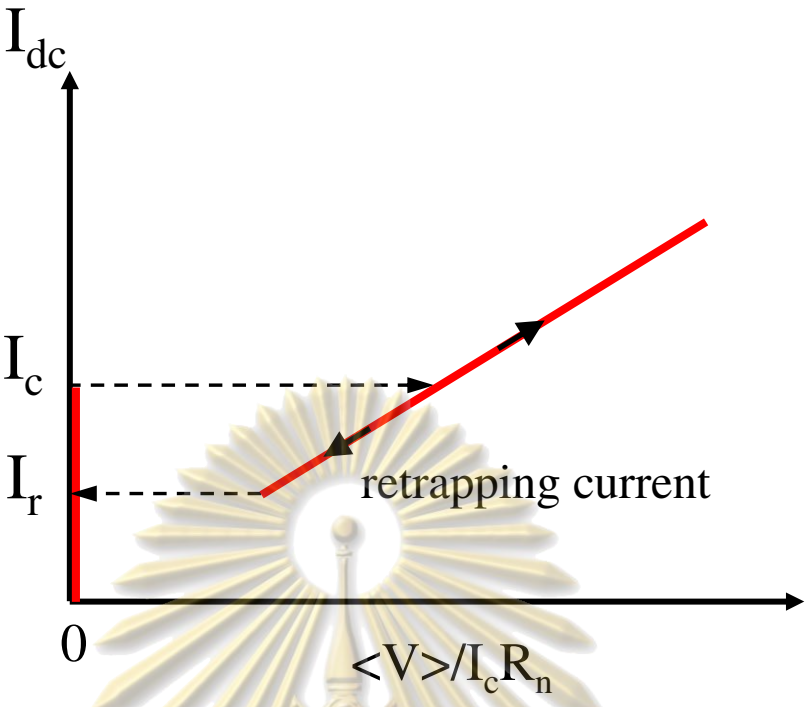

Figure 3.11: The hysteretic curve of I-V characteristic with $\beta > 1$.

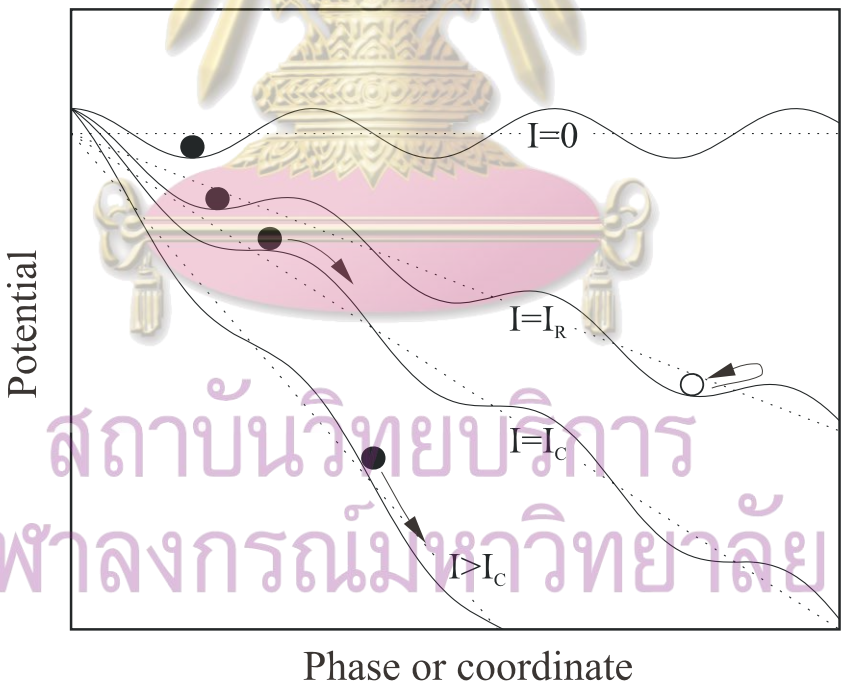

Figure 3.12: Model of a massive particle moving in the tilted washboard potential[14].

3.4 Summary

In this chapter, I have briefly described the theoretical background of Josephson junction and discussed the characteristics of Josephson junction. Then, the RCSJ model was used to describe and explain the classical dynamic of Josephson junction related to the electrical properties of the junction. The current-voltage characteristic of the Josephson junction can be explained by using a model of a particle sliding down the tilted washboard potential. This potential is to be used for investigating the quantum behaviors of the junction. The energy-level quantization in current-biased Josephson junction has been observed since 1985[15]. The calculation of quantum behaviors of the Josepson junction will be described in the next chapter.

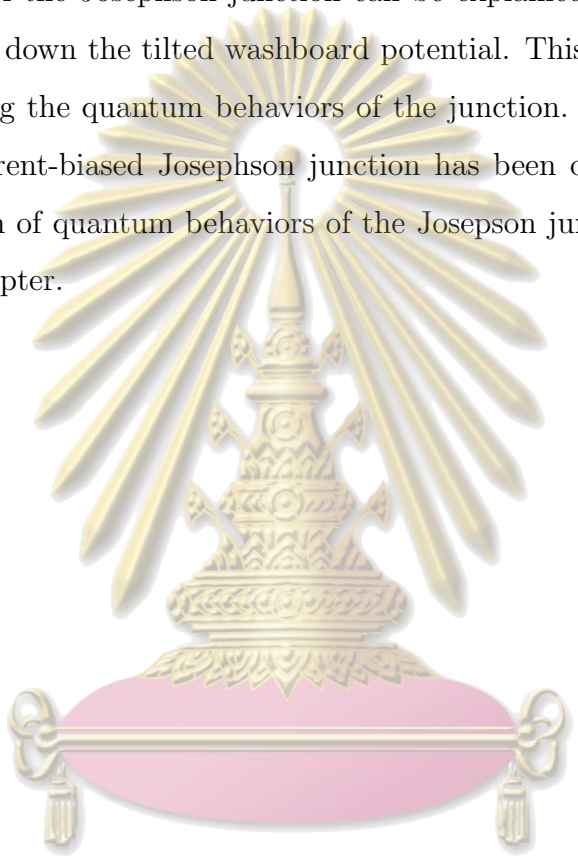

CHAPTER IV

CALCULATION OF QUANTUM BEHAVIORS OF THE JOSEPHSON JUNCTION

In this chapter, I will present the method and the calculation details for finding quantum behaviors of Josephson junction such as the quantized energy levels in the approximation washboard potential, the tunneling rates through the potential barrier, the state wave functions, transition rates between energy levels due to electromagnetic radiation and decoherence times caused by current noise in the junction. This knowledge is very useful for simplifying an experiment and shows that the two-level system of Josephson junction is possible to be used as a quantum bit in quantum computer. The theory of quantum mechanics as well as the semiclassical methods is used to calculate and explain the quantum behaviors.

4.1 The Hamiltonian of the Josephson junction

From the RCSJ model, I have shown how to obtain the effective potential of the Josephson junction system known as the washboard potential. In this section, I will use this potential to find a Hamiltonian of the system. According to the Lagrangian,

$$\begin{aligned} L &= T - U \\ &= \frac{1}{2}CV^2 + \frac{\hbar}{2e}I_c\cos\gamma + \frac{\hbar}{2e}I_{dc}\gamma \\ &= \frac{1}{2}C(\frac{\hbar}{2e})^2\dot{\gamma}^2 + \frac{\hbar}{2e}I_c\cos\gamma + \frac{\hbar}{2e}I_{dc}\gamma, \end{aligned}$$

the kinetic energy of the system is the energy stored in a charged capacitor. From the generalized momenta $p_i = \partial L/\partial \dot{q}_i$, the Hamiltonian can be written as

$$\begin{aligned} H &= p_i\dot{q}_i - L \\ &= \frac{p_\gamma^2}{2m} - \frac{\hbar}{2e}I_c\cos\gamma - \frac{\hbar}{2e}I_{dc}\gamma \\ &= \frac{p_\gamma^2}{2m} - m\omega_0^2\cos\gamma - \frac{\hbar}{2e}I_{dc}\gamma, \end{aligned}$$

where $m = C(\hbar/2e)^2$ is the mass of the system and $\omega_0 = \sqrt{2eI_c/\hbar C}$ is called plasma frequency. The quantum mechanical behaviors can be observed when the bias current is slightly smaller than the critical current $I_{dc} \lesssim I_c$.

4.2 Energy level

The energy-level quantization in the zero-voltage state of a current-biased Josephson junction was directly measured by spectroscopy[15, 16]. In this section, I will show how to calculate the quantized energy levels in the potential well using the semiclassical method known as Bohr Sommerfeld quantization rule. The washboard potential can be approximated by a cubic parabola potential, that is defined by a polynomial function with degree less than or equal to 3, when the applied bias current is close to the critical current. This approximation is helpful in calculating the energy levels and the wave functions because a non-linear term is rather difficult to solve in the differential equation. The potential can be written as

$$U(q) = 3U_0[\frac{q}{q_0}]^2[1 - \frac{2}{3}\frac{q}{q_0}], \tag{4.1}$$

where $q = \gamma - \sin^{-1}I'$, $I' = I_{dc}/I_c$, and $q_0 = 2(1-I'^2)^{1/2}/I'$ is the position of the maximum of the barrier being considered and $U_0 = \hbar I_c(1-I'^2)^{3/2}/3eI'^2$ is the height of the barrier, given in terms of the junction parameters. The cubic potential is shown schematically in Fig. 4.1, where $q_3 = x_3q_0$, $q_2 = x_2q_0$ and $q_1 = x_1q_0$ are the classical turning points at energy E. The calculation details are described in Appendix A.

According to the Bohr Sommerfeld quantization rule for no rigid wall[17], I

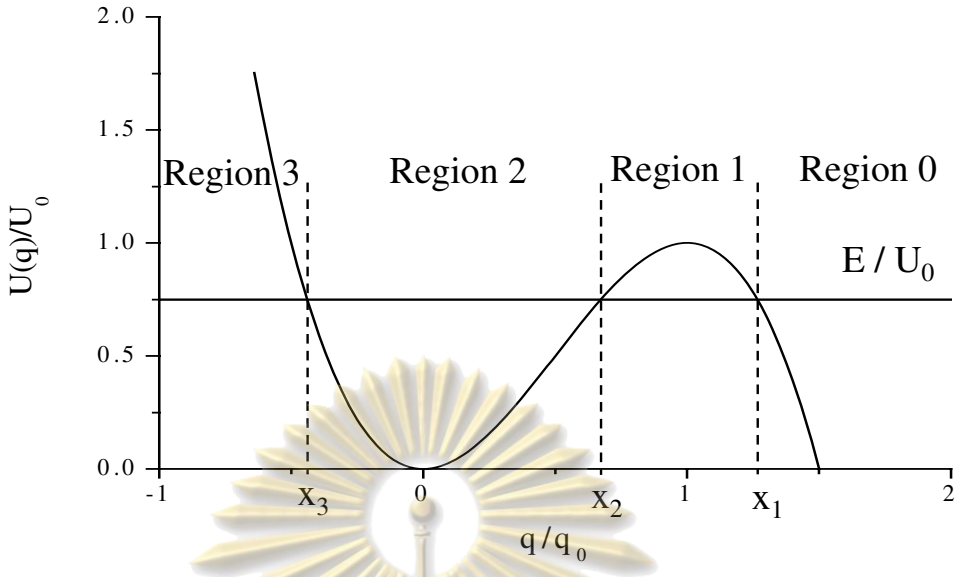

Figure 4.1: The cubic parabola potential.

have

$$\frac{1}{\hbar}\int_{q_3}^{q_2}\sqrt{2m(E-U)}dq = \pi(n+\frac{1}{2}) : n = 0, 1, 2, \dots \ . \tag{4.2}$$

The left hand side of Eq.(4.2) can be written as

$$\begin{aligned}
\int_{q_3}^{q_2}\sqrt{2m(E-U)}dq &= \int_{q_3}^{q_2}\sqrt{2m(E-3U_0[\frac{q}{q_0}]^2[1-\frac{2}{3}\frac{q}{q_0}])}dq \\
&= q_0\int_{x_3}^{x_2}\sqrt{2m(E-3U_0x^2[1-\frac{2}{3}x])}dx \\
&= q_0\sqrt{2mU_0}\int_{x_3}^{x_2}\sqrt{\frac{E}{U_0}-3x^2+2x^3}dx \\
&= 2q_0\sqrt{mU_0}\int_{x_3}^{x_2}\sqrt{x^3-\frac{3}{2}x^2+\frac{E}{2U_0}}dx,
\end{aligned}$$

where $x_3(E) < x_2(E) < x_1(E)$ are the roots of the equation $x^3 - \frac{3}{2}x^2 + \frac{E}{2U_0}$. I can rewrite this equation as

$$x^3 - \frac{3}{2}x^2 + \frac{E}{2U_0} = (x-x_3)(x_2-x)(x_1-x). \tag{4.3}$$

Let $t = (x-x_3)/(x_2-x_3)$; $x = x_{23}t + x_3$; $dx = x_{23}dt$ and $x_{23} = x_2 - x_3$, thus

$$\begin{aligned}
2q_0\sqrt{mU_0}\int_{x_3}^{x_2}\sqrt{x^3-\frac{3}{2}x^2+\frac{E}{2U_0}}dx &= 2q_0\sqrt{mU_0}\int_{x_3}^{x_2}\sqrt{(x-x_3)(x_2-x)(x_1-x)}dx \\
&= 2q_0\sqrt{mU_0}\int_0^1\sqrt{x_{23}t(x_{23}-x_{23}t)(x_{13}-x_{23}t)}dt \\
&= 2q_0\sqrt{mU_0}x_{23}^2x_{13}^{1/2}\int_0^1\sqrt{t(1-t)(1-\frac{x_{23}}{x_{13}}t)}dt.
\end{aligned}$$

Using the integral formula $\int_0^1 x^{\lambda-1}(1-x)^{\mu-1(1-\beta x)^{-\nu}}dx = B(\lambda,\mu)_2F_1(\nu,\lambda;\lambda+\mu;\beta)$ where $B(\lambda,\mu)$ is the beta function (Euler's integral of the first kind)[18] and ${}_2F_1(\nu,\lambda;\lambda+\mu;\beta)$ is the Gaussian hypergeometric function[19], then

$$2q_0\sqrt{mU_0}\int_{x_3}^{x_2}\sqrt{x^3-\frac{3}{2}x^2+\frac{E}{2U_0}}dx = 2q_0\sqrt{mU_0}x_{23}^2x_{13}^{1/2}B(\frac{3}{2},\frac{3}{2})_2F_1(-\frac{1}{2},\frac{3}{2};3;\frac{x_{23}}{x_{13}}). \tag{4.4}$$

Note that beta function is defined by $B(\lambda,\mu) = \int_0^1 t^{\lambda-1}(1-t)^{\mu-1}dt$, therefore $B(\frac{3}{2},\frac{3}{2}) = \int_0^1\sqrt{t(1-t)}dt = \pi/8$. The quantized energy levels calculated by the Bohr Sommerfeld quantization rule are

$$\begin{aligned}\int_{q_3}^{q_2}\sqrt{2m(E-U)}dq &= 2q_0\sqrt{mU_0}x_{23}^2x_{13}^{1/2}(\frac{\pi}{8})_2F_1(-\frac{1}{2},\frac{3}{2};3;\frac{x_{23}}{x_{13}})\\ &= \pi\hbar(n+\frac{1}{2}) : n = 0,1,2,\dots\ .\end{aligned}$$

The energy levels inside the well depend on the junction parameters such as the critical current (I_c) and the capacitance (C) as well as the applied bias current (I_{dc}). When the bias current is raised, the potential well becomes shallow, thus decreasing the number of energy levels. The values of the two energy levels inside the well vs. bias current are shown in Fig. 4.2 and the energy level spacing

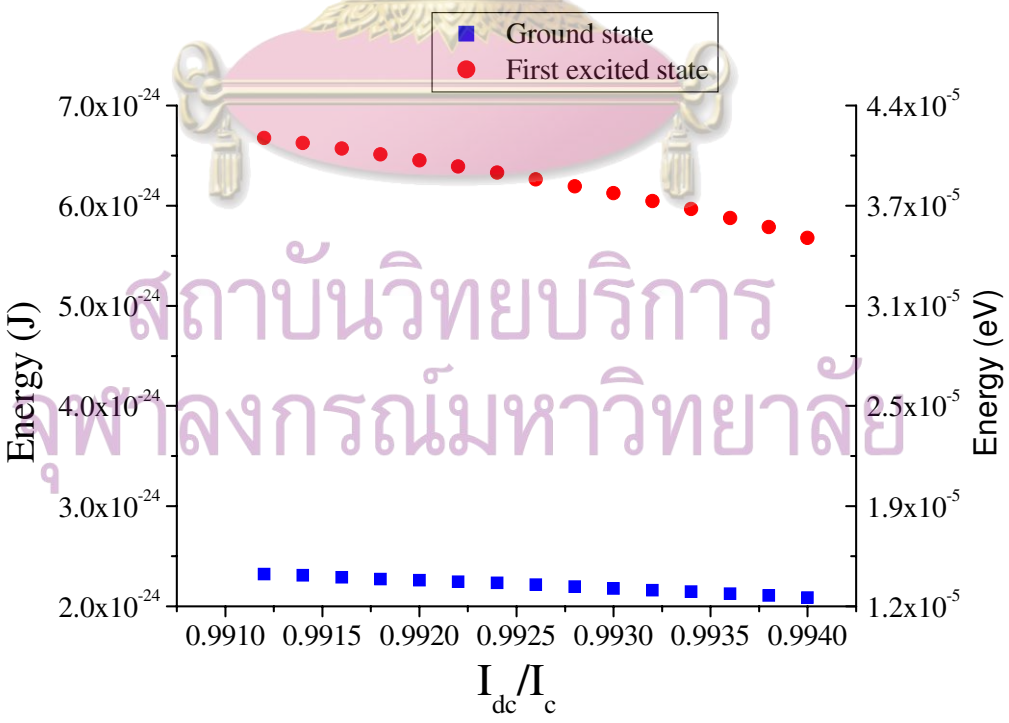

Figure 4.2: The energy levels of ground state and first excited state.

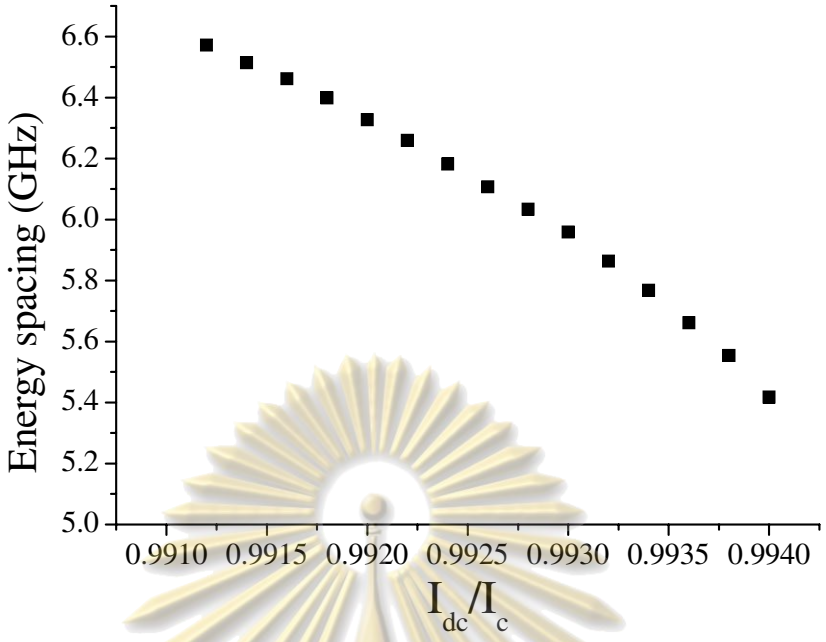

Figure 4.3: The energy levels spacing of ground state and first excited state.

in the range of microwave frequency (GHz) is shown in Fig. 4.3 (the junction parameters are $I_c = 20\mu A$ and $C = 4pF$). A microwave current can be applied as a perturbation to observe the transition between the two lowest lying states. The results agree with the previous result by P. Kopietz et al.[20] but the solution is presented in another function.

4.3 Tunneling rate

Two energy levels of Josephson junction may be used as qubits correspond to bit 1 and 0 respectively by representing the ground state with $|0\rangle$ and the first excited state with $|1\rangle$. However, a quantum effect known as tunneling effect can occur, i.e. a particle can tunnel through the potential barrier as shown in Fig. 4.4. In this section, the tunneling rates at each energy level of the Josephson junction will be calculated using the semiclassical method. According to the WKB formula[21], the tunneling rate from the n^{th} energy level is

$$\Gamma_n = \frac{1}{T(E_n)} \exp(-\frac{2S_f(E_n)}{\hbar}), \tag{4.5}$$

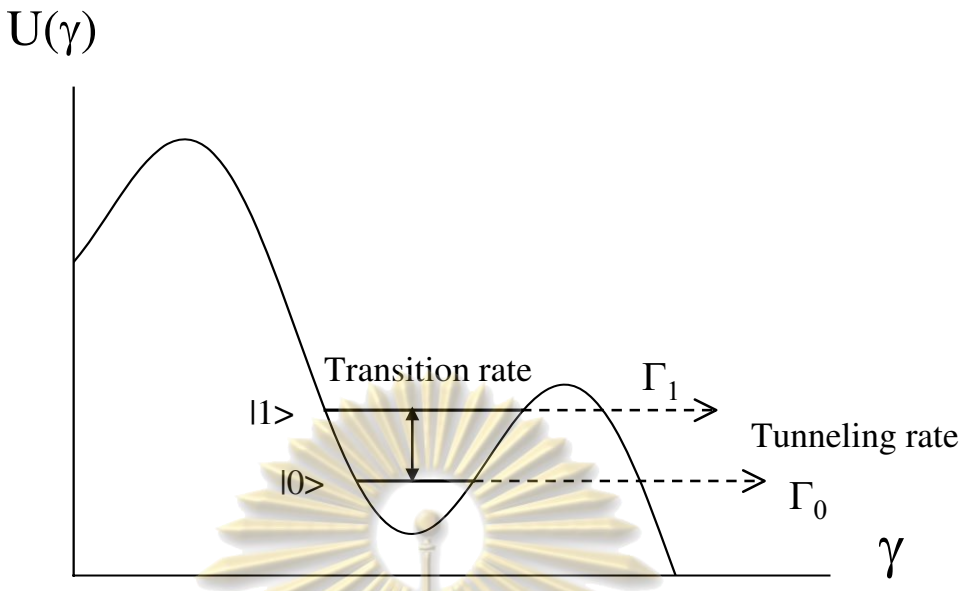

Figure 4.4: The tunneling effect and the transition in the washboard potential.

where $T(E_n)$ is the period of the classical motion at energy E_n, defined by $T(E) = \oint \frac{\partial p}{\partial E} dx = \oint \frac{dx}{v}$. From the momentum $p = \sqrt{(2m(E-U))}$, I obtain

$$\begin{aligned} T(E_n) &= 2\int_{q_2}^{q_1} \frac{m}{\sqrt{2m(U-E_n)}} dq \\ &= q_0\sqrt{\frac{m}{U_0}} \int_{x_2}^{x_1} \frac{dx}{\sqrt{-x^3+\frac{3}{2}x^2-\frac{E_n}{2U_0}}} \\ &= q_0\sqrt{\frac{m}{U_0}} \int_{x_2}^{x_1} \frac{dx}{\sqrt{(x-x_3)(x-x_2)(x_1-x)}}, \end{aligned}$$

and using the integral formula in[19], the period of classical motion is

$$T(E_n) = 2q_0\sqrt{\frac{m}{U_0}} \frac{1}{\sqrt{x_1-x_3}} EllipticK(k), \tag{4.6}$$

where $k = \sqrt{\frac{x_1-x_2}{x_1-x_3}}$ and $EllipticK(k)$ is the complete elliptic integral of the first kind[22]. The Euclidean action across the classically forbidden region (region 1) is

$$\begin{aligned} S_f(E_n) &= \int_{q_2}^{q_1} \sqrt{2m(U-E_n)} dq \\ &= 2q_0\sqrt{mU_0} \int_{x_2}^{x_1} \sqrt{-x^3+\frac{3}{2}x^2-\frac{E_n}{2U_0}} dx \\ &= 2q_0\sqrt{mU_0} \int_{x_2}^{x_1} \sqrt{(x-x_3)(x-x_2)(x_1-x)} dx. \end{aligned}$$

Let $t = \frac{x-x_2}{x_1-x_2}$, $x = x_{12}t + x_2$, and $dx = x_{12}dt$, thus

$$\begin{aligned} S_f(E) &= 2q_0\sqrt{mU_0}\int_0^1 \sqrt{(x_{12}t + x_{23})(x_{12}t)(x_{12} - x_{12}t)}dt \\ &= 2q_0\sqrt{mU_0}x_{12}^2 x_{23}^{1/2}\int_0^1 \sqrt{t(1-t)(1-\frac{x_{12}}{x_{23}}t)}dt. \end{aligned}$$

Using the integral formula $\int_0^1 x^{\lambda-1}(1-x)^{\mu-1(1-\beta x)^{-\nu}}dx = B(\lambda,\mu)_2F_1(\nu,\lambda;\lambda+\mu;\beta)$. The Euclidean action can be written as

$$S_f(E) = 2q_0\sqrt{mU_0}x_{12}^2 x_{23}^{1/2}B(\frac{3}{2},\frac{3}{2})_2F_1(-\frac{1}{2},\frac{3}{2};3;-\frac{x_{12}}{x_{23}}) \quad (4.7)$$

$$= 2q_0\sqrt{mU_0}x_{12}^2 x_{23}^{1/2}(\frac{\pi}{8})_2F_1(-\frac{1}{2},\frac{3}{2};3;-\frac{x_{12}}{x_{23}}). \quad (4.8)$$

The tunneling rate describing the transmission of the particle through the potential barrier is exponentially decay with the action per a period of time. The states at higher energy level are more easily to tunnel through the barrier than the lower states. The transmission coefficients of ground state and first excited state exponentially increase with the bias current as shown in Fig. 4.5. For the energy level near the top of the barrier, the transmission coefficient becomes unity. The tunneling rates of the ground state and the first excited state are shown in Fig. 4.6. It can be seen that the tunneling rates of the first excited state is about 3

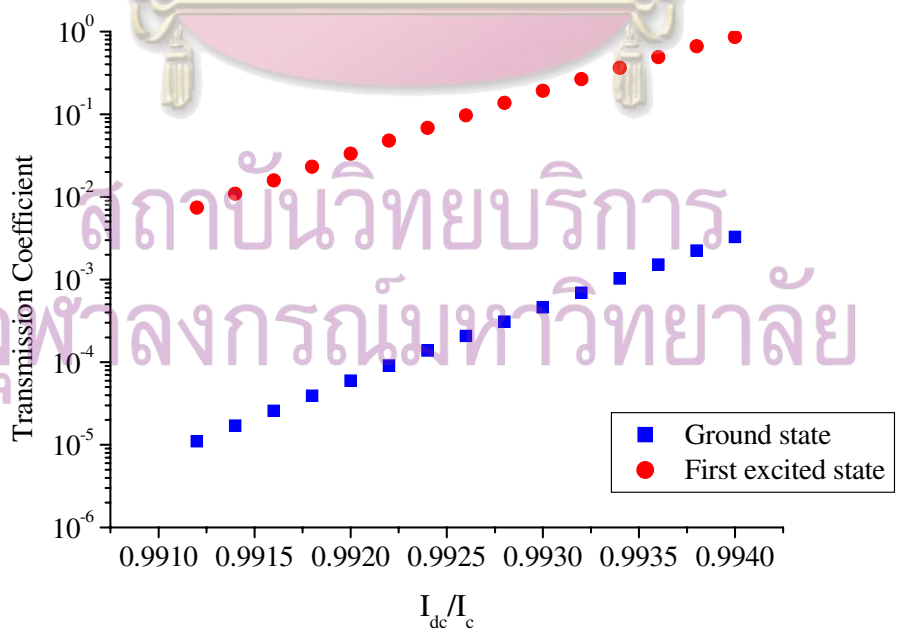

Figure 4.5: The transmission coefficient of ground state and first excited state.

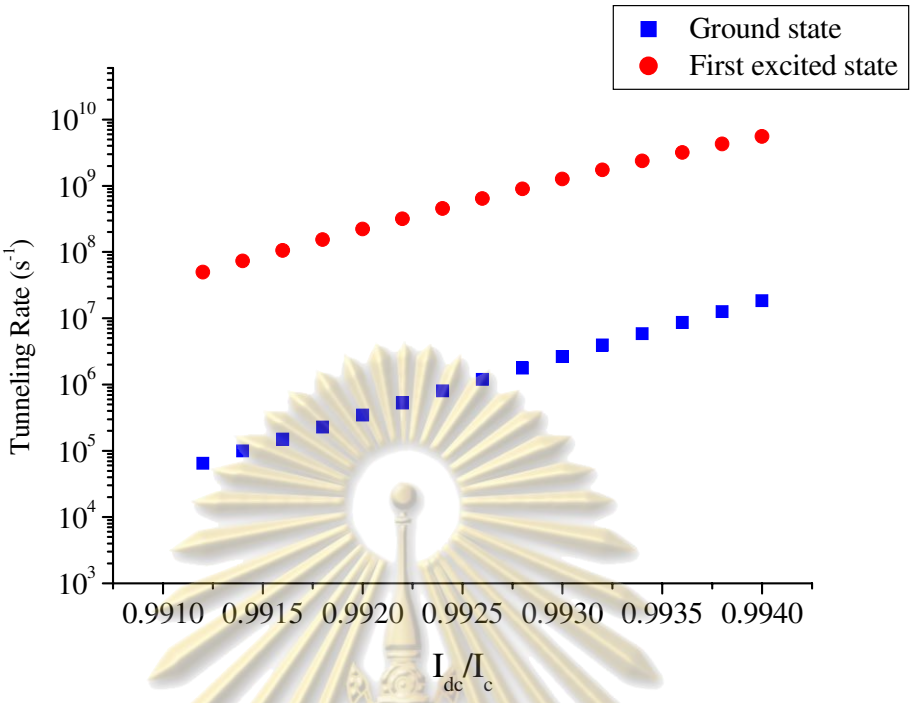

Figure 4.6: The tunneling rate of ground state and first excited state.

orders of magnitude more than that of the ground state. In experiment, if the tunneling occurs, the voltage across the junction will be observed because the particle has a phase difference evolving in time. This is an obstacle for quantum computation because the primary states cannot be kept to perform computation. For the results presented here, the time scale of the ground state of the particle is more than 100 ns before the tunneling occurs. The lifetime of the zero-voltage state can be described by a master equation[20, 23]. This result is equal to the previous work by P. Kopietz *et al.* but the solutions are represented in another function.

4.4 Wave function

In quantum mechanics, the probability of finding a particle can be described and observed the quantum property from the wave function. In this section, I will show how to find the energy levels and the wave functions of the cubic parabola potential by solving the time independent Schrödinger equation numerically. According to

the one dimensional Schrödinger equation

$$-\frac{\hbar^2}{2m}\frac{\partial^2\Psi_n}{\partial x^2}+V(x)\Psi_n=E_n\Psi_n, \tag{4.9}$$

the approximation wave function $(w_j^{(n)})$ is considered in an interval (a,b) under the three conditions[24]

1. $x_j = lj$; $j = 1, 2, 3, ..., N-1$
2. $w_j^{(n)} = \Psi_n(x_j)$
3. $w_0^{(n)} = w_N^{(n)} = 0$ (boundary condition), where $x_0 = a$, $x_N = b$ and l is the step size defined by $l = (b-a)/N$.

The interval of the wave function is divided to N points and the wave function $(\Psi_n(x_j))$ at any point x_j is approximated with approximation wave function $(w_j^{(n)})$, as well as using the boundary condition at the ends of the interval. Following the derivative approximations,

$$\Psi_n''(x_j) \simeq \frac{1}{l^2}\{w_{j-1}^{(n)}-2w_j^{(n)}+w_{j+1}^{(n)}\}, \tag{4.10}$$

$$\Psi_n'(x_j) \simeq \frac{1}{2l}\{w_{j+1}^{(n)}-w_{j-1}^{(n)}\}, \tag{4.11}$$

the approximated wave function can be inserted into the Schrödinger equation, and obtained a system of equations for solving the eigenvalue problem. At the first point $(j = 1)$ on the solution,

$$-\frac{\hbar^2}{2m}\frac{1}{l^2}\{0-2w_1^{(n)}+w_2^{(n)}\}+V(x_1)w_1^{(n)}=E^n w_1^{(n)}, \tag{4.12}$$

at the second point $(j = 2)$ on the solution,

$$-\frac{\hbar^2}{2m}\frac{1}{l^2}\{w_1^{(n)}-2w_2^{(n)}+w_3^{(n)}\}+V(x_2)w_2^{(n)}=E^n w_2^{(n)}, \tag{4.13}$$

and at the last point $(j = N-1)$ on the solution,

$$-\frac{\hbar^2}{2m}\frac{1}{l^2}\{w_{N-2}^{(n)}-2w_{N-1}^{(n)}+0\}+V(x_2)w_{N-1}^{(n)}=E^n w_{N-1}^{(n)}. \tag{4.14}$$

These can be rewritten in a matrix form as a tridiagonal matrix represented by

$$\begin{pmatrix} \frac{\hbar^2}{2m}\frac{2}{l^2}+V(x_1) & -\frac{\hbar^2}{2m}\frac{1}{l^2} & 0 & 0 \\ -\frac{\hbar^2}{2m}\frac{1}{l^2} & \frac{\hbar^2}{2m}\frac{2}{l^2}+V(x_2) & -\frac{\hbar^2}{2m}\frac{1}{l^2} & 0 \\ \vdots & \vdots & \ddots & \vdots \\ 0 & 0 & \cdots & \ddots \end{pmatrix}\begin{pmatrix} w_1^{(n)} \\ w_2^{(n)} \\ \vdots \\ w_{N-1}^{(n)} \end{pmatrix} = E^{(n)}\begin{pmatrix} w_1^{(n)} \\ w_2^{(n)} \\ \vdots \\ w_{N-1}^{(n)} \end{pmatrix}. \tag{4.15}$$

I then need to solve the eigenvalue problem of $(N-1)\times(N-1)$ matrix to obtain the energy eigenvalues and the eigenfunctions of the system. The error of this approximation depend on the step size in $O(l^2)$. This method is applied to the cubic parabola potential. The Schrödinger equation can be rewritten as

$$\begin{aligned} -\frac{\hbar^2}{2m}\frac{\partial^2\Psi_n}{\partial q^2} + 3U_0[\frac{q}{q_0}]^2[1-\frac{2}{3}\frac{q}{q_0}]\Psi_n &= E_n\Psi_n \\ -\frac{\hbar^2}{2mq_0^2}\frac{\partial^2\Psi_n}{\partial x^2} + 3U_0x^2[1-\frac{2}{3}x]\Psi_n &= E_n\Psi_n, \end{aligned}$$

and choose the interval of the wave function $x_0=-1$ and $x_N=2$ by considering the shape of the potential that the wave function vanishes at the ends of the interval. By setting $N=500$, a system of 499 equations is obtained for solving the eigenvalue problem. A large number of energy eigenvalues and eigenfunctions can be found but only the eigenvalues and the eigenfunctions inside the well ($E<U_0$) are interested. The energy eigenvalues is in good agreement with the quantization energies. It was found that the difference never exceed 2 % depending on the number of matrix used as shown in Fig. 4.7 for the first five levels. The numerical wave functions of the first five states are shown in Figs. 4.8-4.12. The wave functions plotted in the cubic parabola potential is shown in Fig. 4.13. It can be seen that they are somewhat similar to the wave functions of the harmonic oscillator because the shape of cubic parabola potential is almost similar to the parabola potential. This result can be used to approximate the operators of this system with the operators of the harmonic oscillator system.

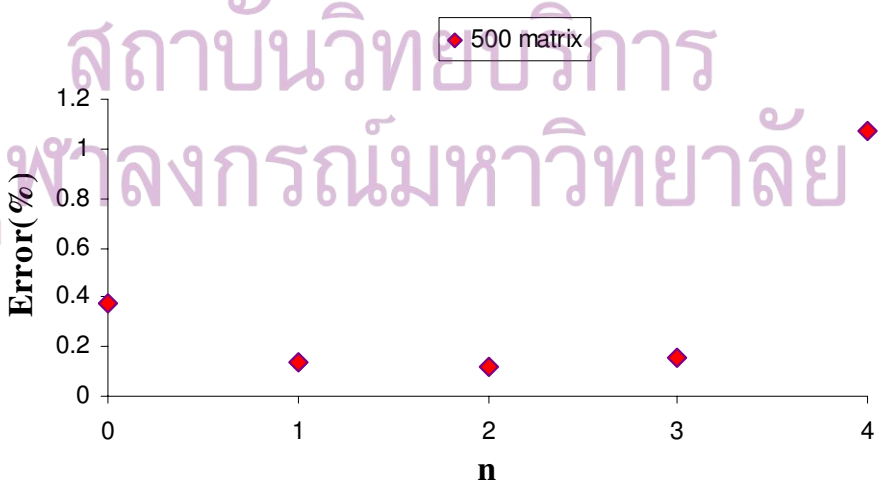

Figure 4.7: The error of the eigen-energy and the quantized energy.

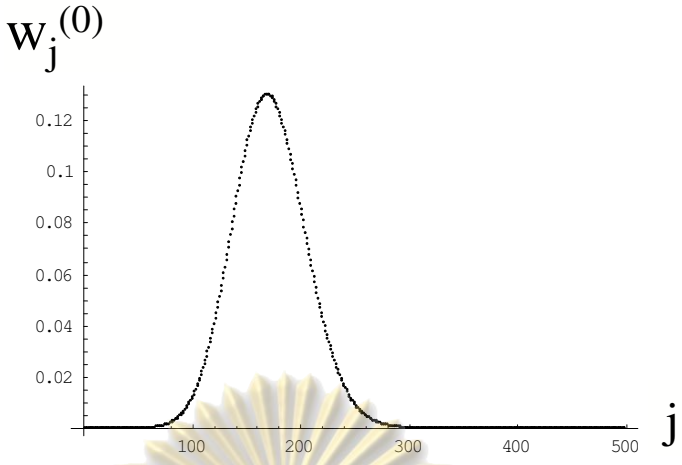

Figure 4.8: The ground state wave function of Josephson junction.

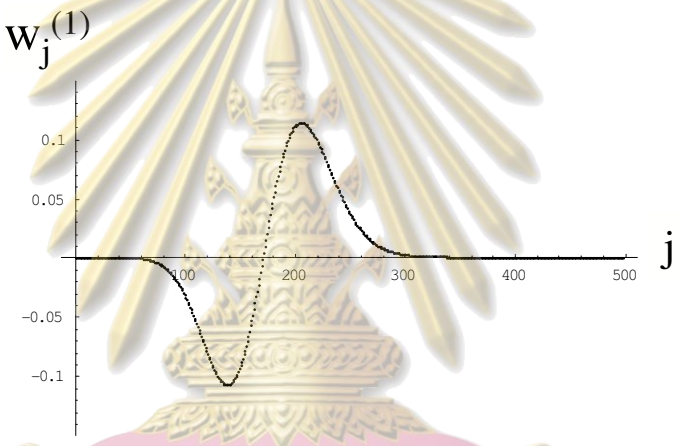

Figure 4.9: The first excited state wave function of Josephson junction.

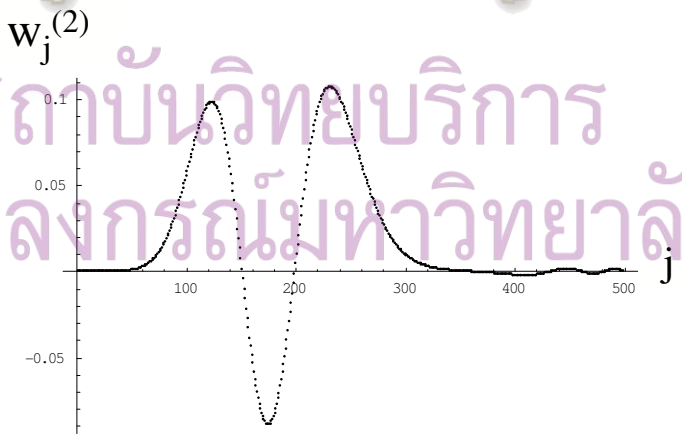

Figure 4.10: The second excited state wave function of Josephson junction.

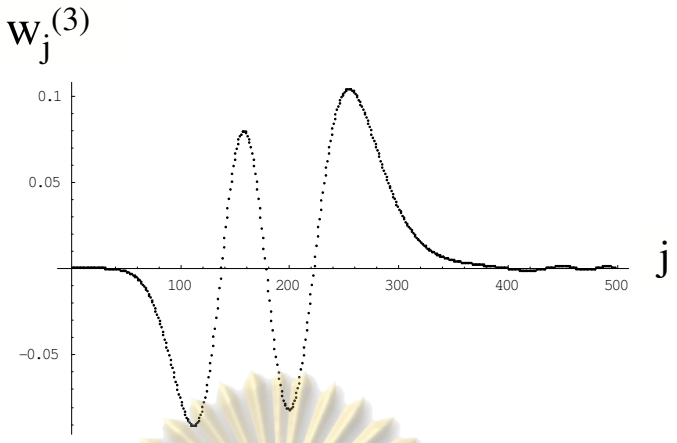

Figure 4.11: The third excited state wave function of Josephson junction.

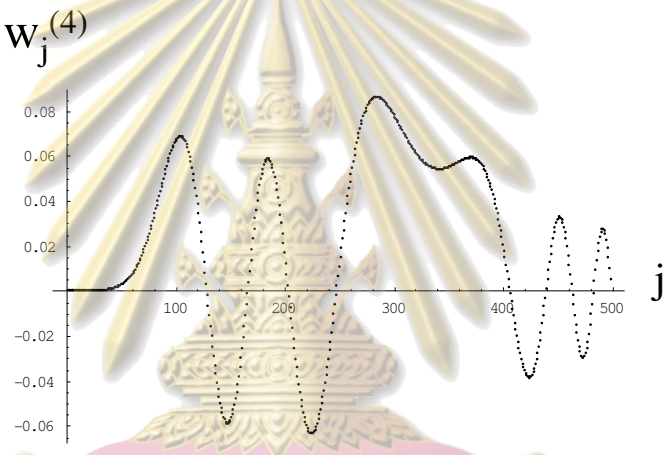

Figure 4.12: The fourth excited state wave function of Josephson junction.

4.5 Transition rate

In this section, I will show how to find the transition rates between the ground state and the first excited state due to an electromagnetic radiation. I first keep only a two-state system and apply the electromagnetic radiation by a microwave current that is an ac current with angular frequency ω as a perturbation. The time-dependent perturbation theory is used to solve the transition rate between the ground state and the first excited state. According to the time-dependent Hamiltonian,

$$H = H^0 + H'(t), \tag{4.16}$$

$$H = \frac{p_\gamma^2}{2m} - \frac{\hbar}{2e}(I_c \cos\gamma + I_{dc}\gamma) - \frac{\hbar}{2e} I_{\mu w}\gamma e^{-i\omega t}, \tag{4.17}$$

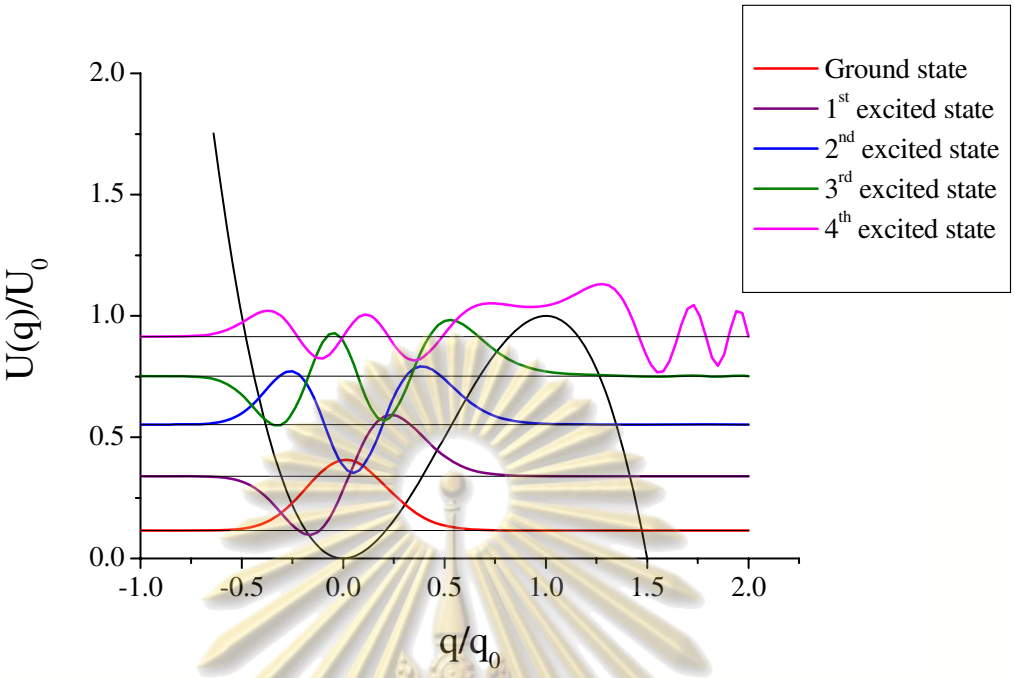

Figure 4.13: The five state wave functions in the cubic parabola potential.

the non-perturbed Hamiltonian can be written in a matrix notation as

$$H^0 = \begin{pmatrix} \langle 0|H^0|0\rangle & \langle 0|H^0|1\rangle \\ \langle 1|H^0|0\rangle & \langle 1|H^0|1\rangle \end{pmatrix} = \begin{pmatrix} E_0 & 0 \\ 0 & E_1 \end{pmatrix}. \tag{4.18}$$

The matrix representation of the perturbed Hamiltonian is $H' = -\frac{\hbar}{2e} I_{\mu w} \hat{\gamma} e^{-i\omega t}$ and can be rewritten as

$$H' = -\frac{\hbar}{2e} I_{\mu w} \begin{pmatrix} 0 & \langle 0|\hat{\gamma}|1\rangle e^{i\omega t} \\ \langle 1|\hat{\gamma}|0\rangle e^{-i\omega t} & 0 \end{pmatrix}, \tag{4.19}$$

where $I_{\mu w}$ is the amplitude of the microwave current. Consider the zero-voltage state of the Josephson junction, the particle sits at the bottom of the well where one may approximate the washboard potential as a harmonic oscillator. The coordinate operator of harmonic oscillator is $\hat{x} = \sqrt{\frac{\hbar}{2m\omega}}(\hat{a} + \hat{a}\dagger)$, where $\omega = \sqrt{k/m}$ is a normal mode of vibration corresponding to the energy $E_n = \hbar\omega(n + \frac{1}{2})$. For the junction system, the ω can be written in terms of energy spacing $(E_1 - E_0)/\hbar = \omega_{10}$. Following this approximation, the matrix element of $\hat{\gamma}$ can be approximated by $\langle 0|\hat{\gamma}|1\rangle = \sqrt{\frac{\hbar}{2m\omega_{10}}}$, where ω_{10} is the frequency corresponding to energy spacing.

The matrix representation of the perturbed Hamiltonian is

$$H' = -\sqrt{\frac{\hbar}{2C\omega_{10}}} I_{\mu w} \begin{pmatrix} 0 & e^{i\omega t} \\ e^{-i\omega t} & 0 \end{pmatrix} = \varepsilon \begin{pmatrix} 0 & e^{i\omega t} \\ e^{-i\omega t} & 0 \end{pmatrix}. \tag{4.20}$$

The state of the two-level system can be written in a superposition of the basis states $|0\rangle$ and $|1\rangle$, given by

$$|\Psi(t)\rangle = e^{-iE_0 t/\hbar} c_0(t)|0\rangle + e^{-iE_1 t/\hbar} c_1(t)|1\rangle, \tag{4.21}$$

or rewritten in a matrix notation as

$$|\Psi(t)\rangle = \begin{pmatrix} e^{-iE_0 t/\hbar} c_0(t) \\ e^{-iE_1 t/\hbar} c_1(t) \end{pmatrix}. \tag{4.22}$$

According to the Schrödinger equation, $i\hbar \frac{d|\Psi(t)\rangle}{dt} = H|\Psi(t)\rangle$, finding the exact solution of the probabilities $c_0(t)$ and $c_1(t)$ will explain the transition between the two energy levels due to the applied microwave current by substituting the full Hamiltonian and the state wave function into the Schrödinger equation, the left hand side, one obtains

$$i\hbar \frac{d|\Psi(t)\rangle}{dt} = i\hbar \begin{pmatrix} -\frac{iE_0}{\hbar} e^{-iE_0 t/\hbar} c_0(t) + e^{-iE_0 t/\hbar} \dot{c_0}(t) \\ -\frac{iE_1}{\hbar} e^{-iE_1 t/\hbar} c_1(t) + e^{-iE_1 t/\hbar} \dot{c_1}(t) \end{pmatrix},$$

and on the right hand side, one obtains

$$H|\Psi(t)\rangle = \begin{pmatrix} E_0 e^{-iE_0 t/\hbar} c_0(t) + \varepsilon e^{i\omega t} e^{-iE_1 t/\hbar} c_1(t) \\ E_1 e^{-iE_1 t/\hbar} c_1(t) + \varepsilon e^{-i\omega t} e^{-iE_0 t/\hbar} c_0(t) \end{pmatrix}.$$

The matrix equation is in the form of

$$\begin{pmatrix} e^{-iE_0 t/\hbar} i\hbar \dot{c_0}(t) \\ e^{-iE_1 t/\hbar} i\hbar \dot{c_1}(t) \end{pmatrix} = \begin{pmatrix} \varepsilon e^{i\omega t} e^{-iE_1 t/\hbar} c_1(t) \\ \varepsilon e^{-i\omega t} e^{-iE_0 t/\hbar} c_0(t) \end{pmatrix}.$$

Thus the two ordinary differential equations are given by

$$i\hbar \dot{c_0}(t) = \varepsilon e^{i\omega t} e^{-i(E_1 - E_0)t/\hbar} c_1(t), \tag{4.23}$$

$$i\hbar \dot{c_1}(t) = \varepsilon e^{-i\omega t} e^{i(E_1 - E_0)t/\hbar} c_0(t). \tag{4.24}$$

Let $(E_1 - E_0)/\hbar = \omega_{10}$ and substitute it into the differential equations,

$$i\hbar \dot{c_0}(t) = \varepsilon e^{i(\omega - \omega_{10})t} c_1(t),$$

$$i\hbar \dot{c_1}(t) = \varepsilon e^{-i(\omega - \omega_{10})t} c_0(t).$$

From Eq.(4.24), the probability $c_0(t)$ is related to the probability $c_1(t)$ by

$$c_0(t) = \frac{1}{\varepsilon} e^{i(\omega-\omega_{10})t} i\hbar \dot{c_1}(t).$$

Differentiating $c_0(t)$ and inserting it into Eq.(4.23), one obtains a second-order differential equation of $c_1(t)$ as

$$\ddot{c_1}(t) + i(\omega - \omega_{10})\dot{c_1}(t) + \frac{\varepsilon^2}{\hbar^2} = 0. \tag{4.25}$$

The differential equation is solved by using the standard technique. Considering $c_1(t) \propto e^{i\alpha t}$, the differential equation becomes

$$\begin{aligned} -\alpha^2 - (\omega - \omega_{10})\alpha + \frac{\varepsilon^2}{\hbar^2} &= 0 \\ \alpha &= \frac{(\omega - \omega_{10}) \pm \sqrt{(\omega - \omega_{10})^2 + 4\varepsilon^2/\hbar^2}}{-2}. \end{aligned}$$

The general solution of the differential equation can be written as

$$c_1(t) = A_1 e^{i\alpha_1 t} + A_2 e^{i\alpha_2 t}, \tag{4.26}$$

where $\alpha_1 = \frac{-(\omega-\omega_{10})-\sqrt{(\omega-\omega_{10})^2+4\varepsilon^2/\hbar^2}}{2}$, $\alpha_2 = \frac{-(\omega-\omega_{10})+\sqrt{(\omega-\omega_{10})^2+4\varepsilon^2/\hbar^2}}{2}$ and A_1, A_2 are constants. From the relation between $c_0(t)$ and $c_1(t)$, The general solution of $c_0(t)$ is

$$c_0(t) = -\frac{\hbar}{\varepsilon} e^{i(\omega-\omega_{10})t}(A_1\alpha_1 e^{i\alpha_1 t} + A_2\alpha_2 e^{i\alpha_2 t}). \tag{4.27}$$

The initial conditions of the state are given by $c_0(0) = 1$ and $c_1(0) = 0$, that the system starts out from the ground state. Following these conditions, the constants A_1 and A_2 can be obtained by

$$\begin{aligned} c_1(0) &= A_1 + A_2 = 0 \\ c_0(0) &= -\frac{\hbar}{\varepsilon}(A_1\alpha_1 + A_2\alpha_2) = 1 \\ A_1 &= -A_2 = \frac{\varepsilon/\hbar}{\sqrt{(\omega - \omega_{10})^2 - 4\varepsilon^2/\hbar^2}}. \end{aligned}$$

The final solutions of differential equation are

$$\begin{aligned} c_0(t) &= e^{\frac{i}{2}(\omega-\omega_{10})t}\{\frac{-i(\omega - \omega_{10})}{\sqrt{(\omega - \omega_{10})^2 + 4\varepsilon^2/\hbar^2}} \sin(\frac{1}{2}\sqrt{(\omega - \omega_{10})^2 + 4\varepsilon^2/\hbar^2}t) \\ &\quad + \cos(\frac{1}{2}\sqrt{(\omega - \omega_{10})^2 + 4\varepsilon^2/\hbar^2}t), \end{aligned}$$

$$c_1(t) = -ie^{-\frac{i}{2}(\omega-\omega_{10})t}\frac{2\varepsilon/\hbar}{\sqrt{(\omega-\omega_{10})^2+4\varepsilon^2/\hbar^2}}\sin(\frac{1}{2}\sqrt{(\omega-\omega_{10})^2+4\varepsilon^2/\hbar^2}t). \quad (4.28)$$

When the microwave current is applied at a resonance frequency, i.e. $\omega = \omega_{10}$, the transition probability will oscillate between zero and unity with the frequency $I_{\mu w}/\sqrt{2\hbar\omega_{10}C}$ as shown in Figs. 4.14 and 4.15. This frequency is known as "Rabi frequency" and the probability $|c_1|^2$ and $|c_0|^2$ are given by

$$|c_1(t)|^2 = \sin^2\frac{I_{\mu w}}{\sqrt{2\hbar\omega_{10}C}}t, \quad (4.29)$$

$$|c_0(t)|^2 = \cos^2\frac{I_{\mu w}}{\sqrt{2\hbar\omega_{10}C}}t. \quad (4.30)$$

The period of the oscillation depends on the amplitude of the microwave current and the energy spacing between the ground state and the first excited state. A least time used in the transition from the ground state to the first excited state is

$$t = \frac{\pi\sqrt{\hbar\omega_{10}C/2}}{I_{\mu w}}.$$

This time corresponds to a gate time used to perform qubit. Considering the frequency of the microwave current, the transition probability is sharply maximum at the resonance frequency ω_{10} and decreases rapidly when the microwave frequency shifts from the resonance frequency as shown in Fig. 4.16 where Ω_i is the i^{th}

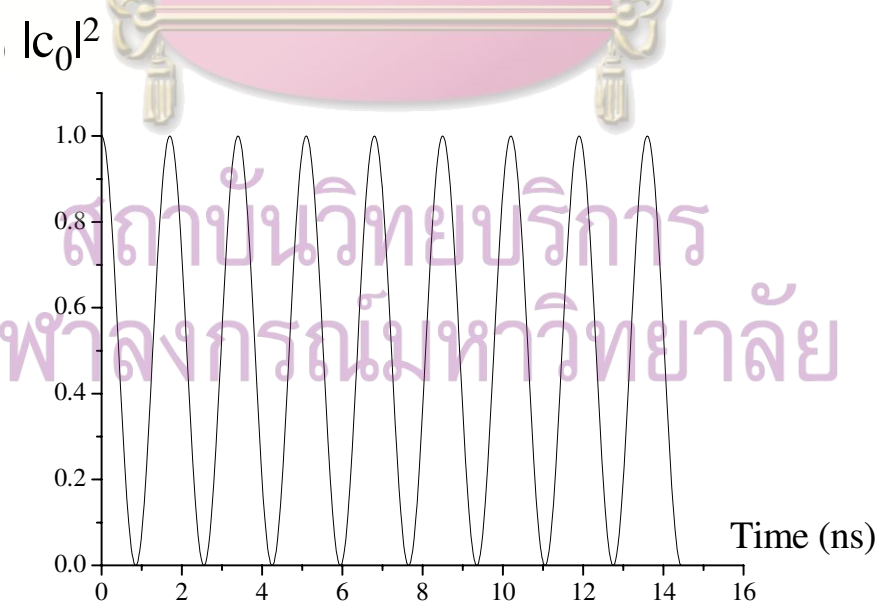

Figure 4.14: The ground state probability when applied a microwave radiation.

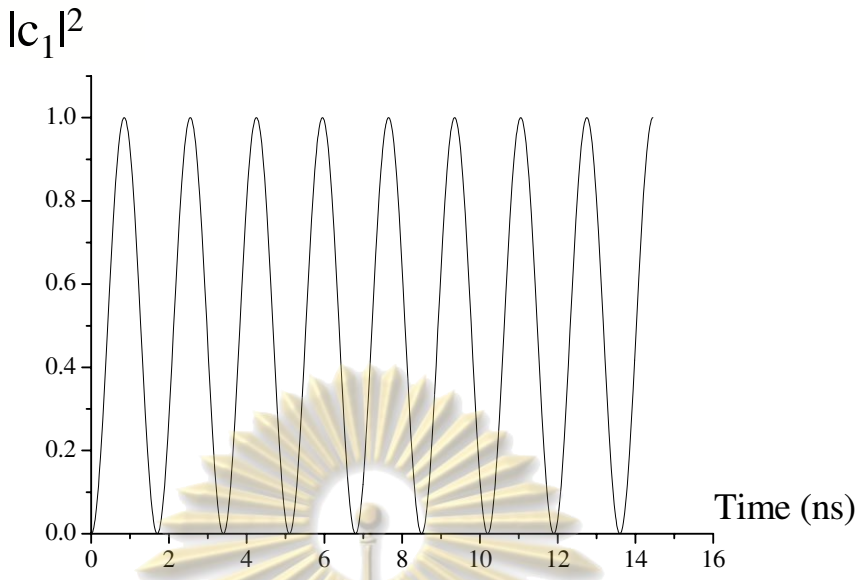

Figure 4.15: The first excited state probability when applied a microwave radiation.

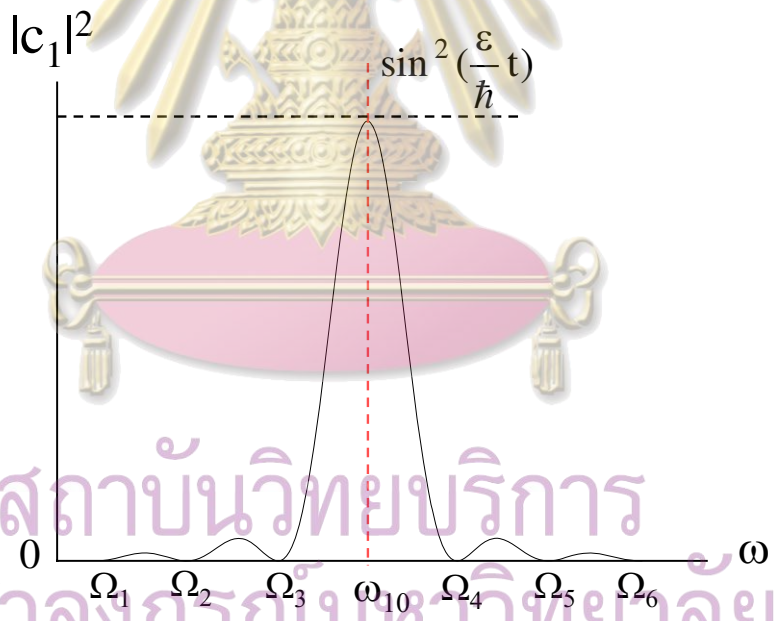

Figure 4.16: The transition probability for a fixed time t by considering the frequency of microwave current.

minimum point of the transition probability. The rate of the transition is considered when t is large. The transition rate can be calculated from the transition probability per unit time defined by

$$\Gamma(i \to j) = \lim_{t\to\infty} \frac{P(i \to j, t)}{t}. \tag{4.31}$$

Considering for a small perturbation where $2I_{\mu w}^2/\hbar\omega_{10}C \ll (\omega - \omega_{10})^2$. The transition rate is given by

$$\Gamma(0 \to 1) = \lim_{t\to\infty} \frac{2I_{\mu w}^2/\hbar\omega_{10}C}{(\omega - \omega_{10})^2 t} \sin^2(\omega - \omega_{10})t/2. \tag{4.32}$$

By using the approximation, $\lim_{t\to\infty} \sin^2 yt/\pi y^2 t$, the final result of transition rate is

$$\Gamma(0 \to 1) = \frac{\pi I_{\mu w}^2 t}{\omega_{10} C} \delta(\hbar(\omega - \omega_{10})). \tag{4.33}$$

The transition rate is maximum at the frequency of microwave current equal to the frequency of the energy spacing as expected.

4.6 Decoherence time

In the previous work of P. Kopietz and S. Chakravarty[20], the dissipation in Josephson junction can be explained by using a quantum statistical technique, a master equation, to describe the density of states under an influence of the environment. The escape rate from a zero voltage state is calculated from the master equation[20]. In quantum computation, qubit operations are performed under the environmental interactions that affect states of the qubits. For the Josephson junction, noise current is one of the cause of decoherence in the qubit. In this section, I introduce a model for calculating a decoherence time in the Josephson junction due to the current noise using the time dependent perturbation theory. Similar to the previous section, the Rabi's oscillations of the two-state system under the influence of the noise current are being interested and used observe a decay of the probability of the states. The microwave current and noise current are applied as the perturbations to the system. According to the time-dependent Hamiltonian,

$$H = H^0 + H'(t), \tag{4.34}$$

$$H = \frac{p_\gamma^2}{2m} - \frac{\hbar}{2e}(I_c \cos\gamma + I_{dc}\gamma) - \frac{\hbar}{2e} I_{\mu w}\gamma e^{-i\omega_{10}t} - \frac{\hbar}{2e} I_{noise}(t)\gamma. \tag{4.35}$$

The perturbed Hamiltonian can be written in a matrix form as

$$H' = \begin{pmatrix} \frac{I_n(t)}{2}(\frac{\partial E_{10}}{\partial I_{dc}}) & I_{\mu w}\sqrt{\frac{\hbar}{2C\omega_{10}}}e^{i\omega_{10}t} \\ I_{\mu w}\sqrt{\frac{\hbar}{2C\omega_{10}}}e^{-i\omega_{10}t} & -\frac{I_n(t)}{2}(\frac{\partial E_{10}}{\partial I_{dc}}) \end{pmatrix}, \tag{4.36}$$

where E_{10} is the energy spacing between the ground state and the first excited state, $I_n(t)$ is a gaussian random noise and $I_{\mu w}$ is the amplitude of microwave current with the resonance frequency ω_{10}. I assume that the noise current causes an energy shift of the ground state and the first excited state. From the section 4.2, it was shown that the energy spacing (E_{10}) depends on the bias current (I_{dc}) as shown in Fig. 4.3. If a noise current is added to the junction, the total bias current ($I_{dc}+I_n$) will change the value of energy spacing. The energy shift term of the ground state and the first excited state is given by the term $\frac{I_n(t)}{2}(\frac{\partial E_{10}}{\partial I_{dc}})$. Note that, the opposite sign refers to the increasing and the decreasing of the energy level. In the interaction picture, the Hamiltonian of system can be written as

$$\begin{aligned} H &= H^0 + H' \\ H &= \begin{pmatrix} E_0 + \frac{I_n(t)}{2}(\frac{\partial E_{10}}{\partial I_{dc}}) & I_{\mu w}\sqrt{\frac{\hbar}{2C\omega_{10}}}e^{i\omega_{10}t} \\ I_{\mu w}\sqrt{\frac{\hbar}{2C\omega_{10}}}e^{-i\omega_{10}t} & E_1 - \frac{I_n(t)}{2}(\frac{\partial E_{10}}{\partial I_{dc}}) \end{pmatrix}, \end{aligned}$$

and the state of the two-level system can be written in a superposition of basis states $|0\rangle$ and $|1\rangle$, given by

$$\begin{aligned} |\Psi(t)\rangle &= e^{-iE_0t/\hbar}c_0(t)|0\rangle + e^{-iE_1t/\hbar}c_1(t)|1\rangle, \\ |\Psi(t)\rangle &= \begin{pmatrix} e^{-iE_0t/\hbar}c_0(t) \\ e^{-iE_1t/\hbar}c_1(t) \end{pmatrix}. \end{aligned}$$

According to the Schrödinger equation, $i\hbar\frac{d|\Psi(t)\rangle}{dt} = H|\Psi(t)\rangle$, inserting the Hamiltonian and the state of qubit into the Schrödinger equation, one obtains two ordinary differential equations

$$i\hbar\dot{c_0}(t) = \frac{I_n(t)}{2}(\frac{\partial E_{10}}{\partial I_{dc}})c_0(t) + I_{\mu w}\sqrt{\frac{\hbar}{2C\omega_{10}}}c_1(t), \tag{4.37}$$

$$i\hbar\dot{c_1}(t) = -\frac{I_n(t)}{2}(\frac{\partial E_{10}}{\partial I_{dc}})c_1(t) + I_{\mu w}\sqrt{\frac{\hbar}{2C\omega_{10}}}c_0(t). \tag{4.38}$$

The 2^{nd} order Runge-Kutta method, i.e. midpoint method as described in Appendix B, is used to solve the system of differential equations. A set of random

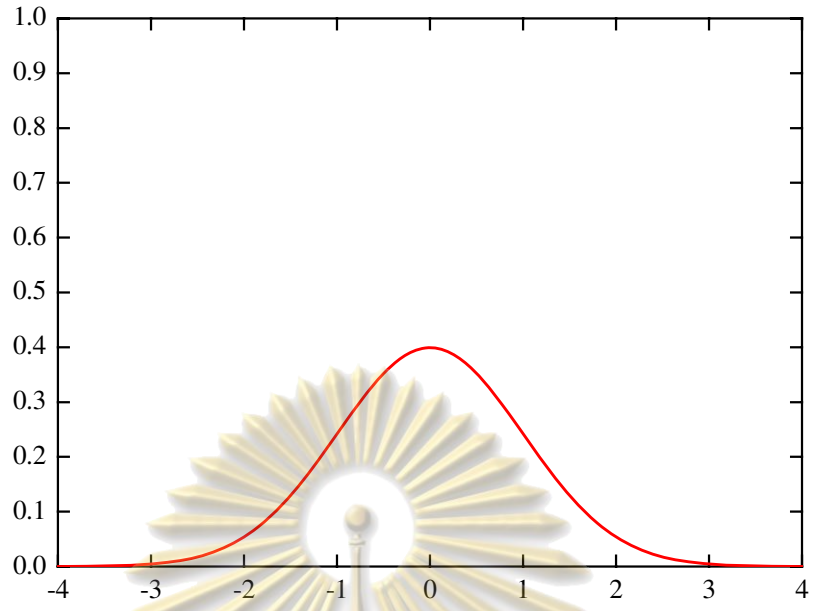

Figure 4.17: The probability density function of the normal distribution.

number is generated using a normal distribution with a standard deviation of one as shown in Fig. 4.17, and define the noise current function by

$$I_n(t) = I_A \exp(-i|R(t)|), \tag{4.39}$$

where I_A is an amplitude of noise current and $R(t)$ is a random number at any time. Inserting the parameters into the differential equations, one obtains

$$\dot{c_0}(t) = \frac{1}{i\hbar}[\frac{I_A}{2}(\frac{\partial E_{10}}{\partial I_{dc}})e^{-i|R(t)|}c_0(t) + I_{\mu w}\sqrt{\frac{\hbar}{2C\omega_{10}}}c_1(t)] \tag{4.40}$$

$$\dot{c_1}(t) = \frac{1}{i\hbar}[-\frac{I_A}{2}(\frac{\partial E_{10}}{\partial I_{dc}})e^{i|R(t)|}c_1(t) + I_{\mu w}\sqrt{\frac{\hbar}{2C\omega_{10}}}c_0(t)], \tag{4.41}$$

or rewrites in a simple form as

$$\frac{dc_0}{dt} = f(t, c_0, c_1)$$
$$\frac{dc_1}{dt} = g(t, c_0, c_1).$$

The initial conditions of the state is chosen by $c_0(0) = 1$ and $c_1(0) = 0$ that the system starts out from the ground state and evolves in time. Then I calculate the transition between the ground state and the first excited state under the influence of the noise current. The numerical solutions of the probability $|c_0(t)|^2$ and $|c_1(t)|^2$ are shown in Figs. 4.18 and 4.19, respectively. It can be seen that the probability

of $|c_0(t)|^2$ and $|c_1(t)|^2$ oscillate (Rabi's oscillation) and exponentially decay with time t in the order of nanoseconds. From the previous section, It was shown that the oscillation frequency depended on the amplitude of the microwave current. Now I am interested in the amplitude of the noise current that cause the decay of the Rabi's oscillation. When the noise current increases, the probability of finding the state decays faster and the decoherence time becomes shorter as shown in Table. 4.1.

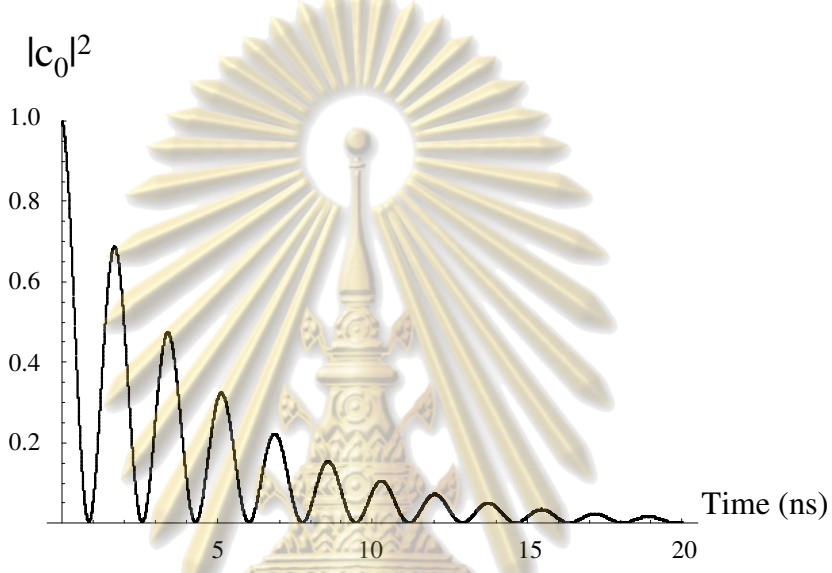

Figure 4.18: The probability of $|c_0|^2$ when perturbing with the current noise.

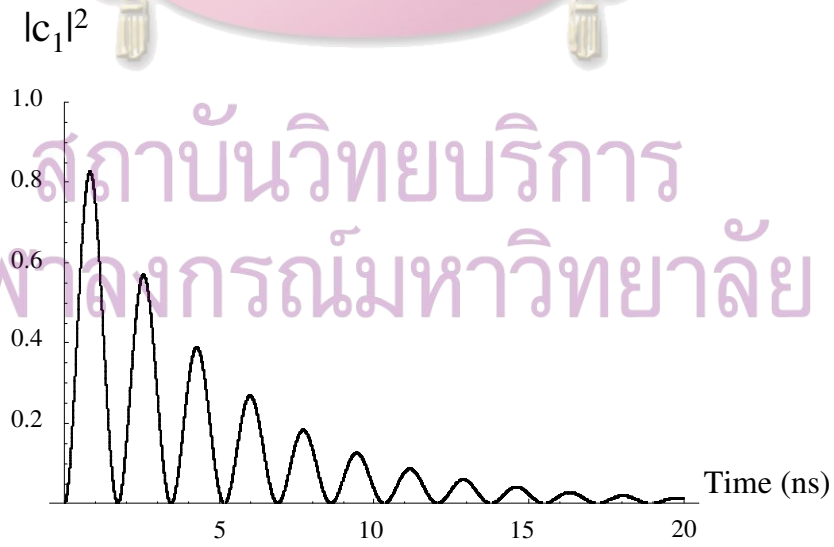

Figure 4.19: The probability of $|c_1|^2$ when perturbing with the current noise.

Noise current(nA)	Decoherence time(ns)
1	21
5	4.2
10	2.0
15	1.4
20	1.0

Table 4.1: The decoherence time in Josephson junction with noise current

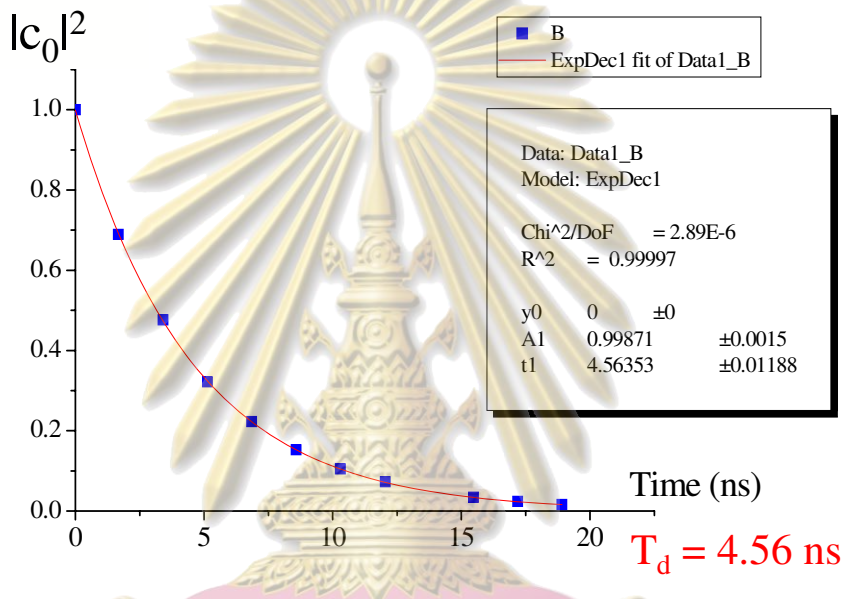

Figure 4.20: The exponential envelop of the probability of $|c_1|^2$ for finding the decoherence time.

Here, the decoherence time is defined as the time when the amplitude of the envelop of the probability reduces by $1/e \approx 0.37$. For example, a 10 nA of the noise current, the decoherence time is about 4 ns as shown in Fig. 4.20. This result is a good agreement with the experimental work by A. J. Berkley *et al.* as shown in Fig. 4.21[25]. The energy spacing with the number of energy levels is shown in Fig. 4.22 for calculating the decoherence time and the decoherence time with the bias current is shown in Fig. 4.23. This suggests that if one wants a longer decoherence time, one must reduce the noise current in the system. For an example, for the decoherence time of 1 μs, one must reduce the noise current to the order of 10 pA.

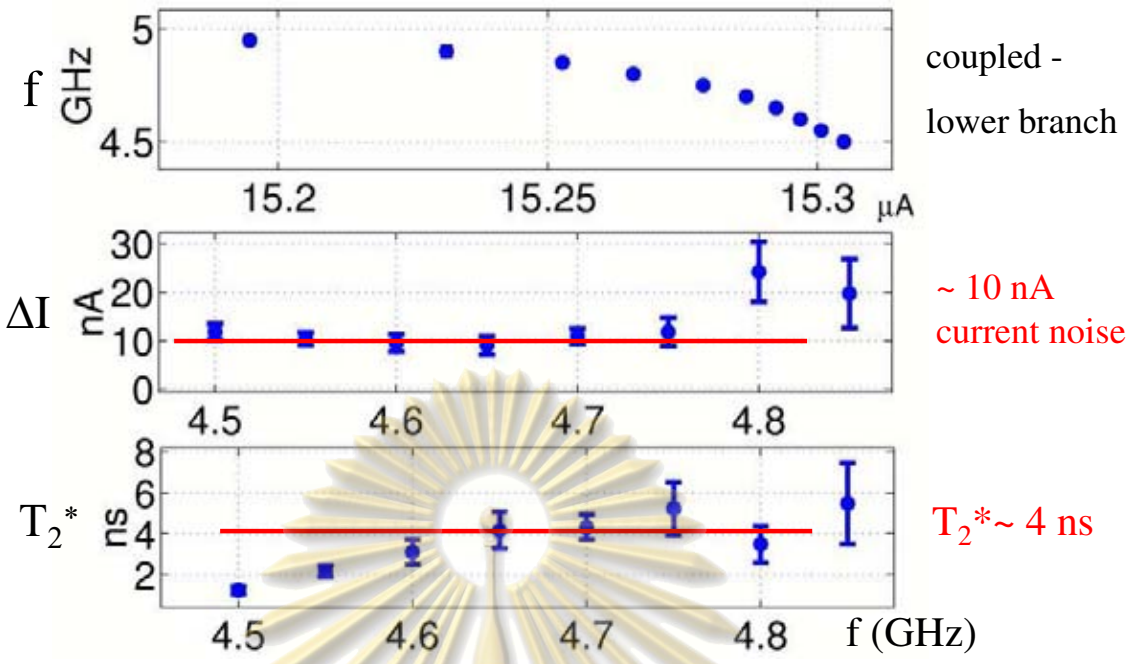

Figure 4.21: The experimental results of the energy spacing, the amplitude of current noise and the decoherence time[25].

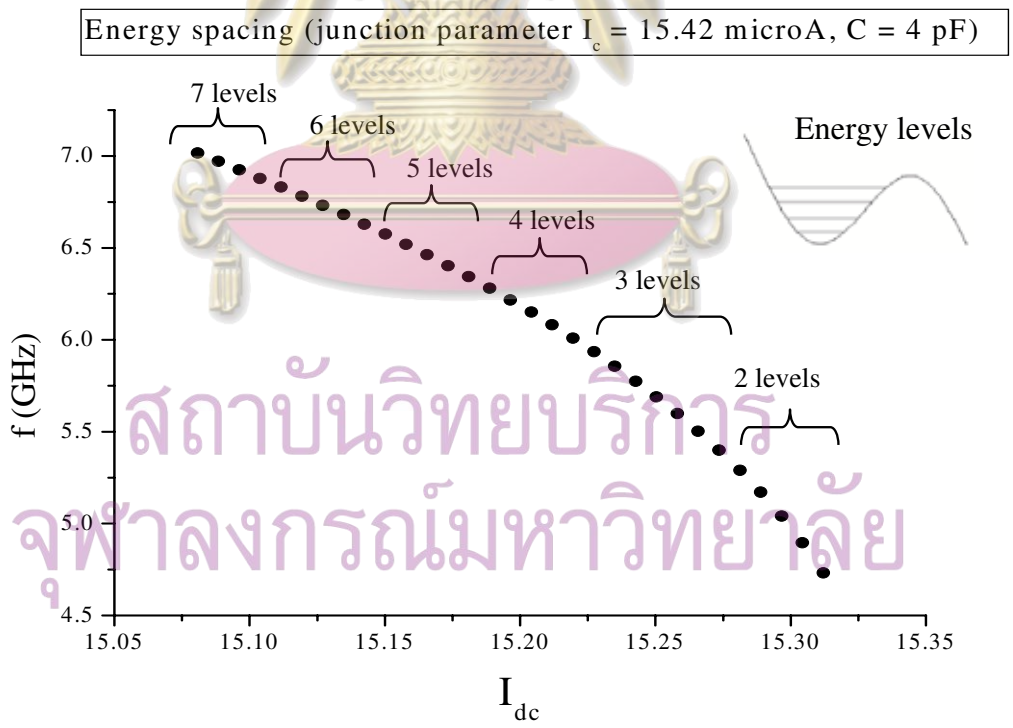

Figure 4.22: The energy spacing and the number of energy levels.

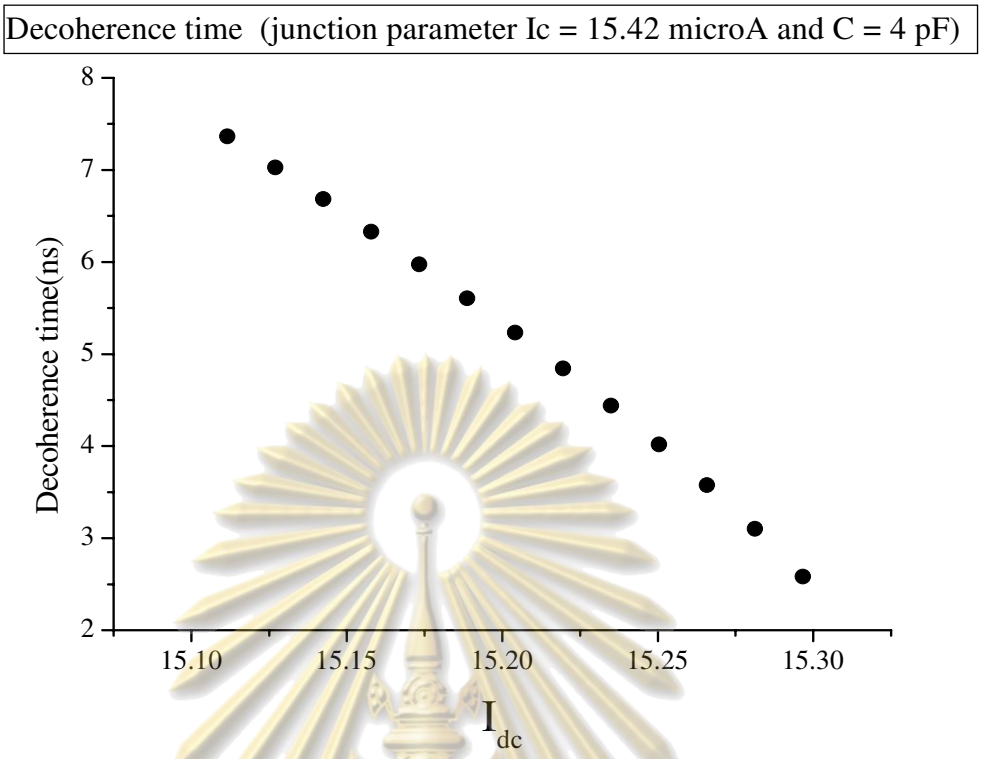

Figure 4.23: The decoherence time with the bias current.

4.7 Summary

In this chapter I present how to calculate the quantum behaviors of the Josephson junction such as energy levels, tunneling rates, wave functions, transition rates and decoherence times. The energy levels in the approximated washboard potential are quantized by using the Bohr-Sommerfeld quantization rule and thus used as a qubit in quantum computation. Then, I calculate the tunneling rates at each energy level and showed the state wave functions in the potential well. Finally, I discuss the external perturbations such as a microwave current and a noise current, that affect states of the qubits. The microwave current causes the transition between energy levels and the noise current causes the decoherence times in the junction.

CHAPTER V

CONCLUSIONS

In this thesis, the characteristic and quantum properties of Josephson junction have been studied. They are necessary for using the Josephson junction as a quantum bit. The mathematical methods and the approximation method in quantum mechanics are used to calculate and describe the behavior of the Josephson junction. The classical dynamic of the Josephson junction can be solved from the classical equation of motion for describing the electrical property of the Josephson junction. It was found that the I-V characteristic of Josephson junction could be hysteretic and the retrapping current depended on the damping parameter of the junction. In the quantum regime, the tilted washboard potential was used to study the quantum behaviors of the Josephson junction. By using Bohr-Sommerfeld quantization rule, the energy levels in the potential well can be quantized and thus used the two-energy levels as a quantum bit in a quantum computer. The number of energy levels inside the well decreases when the bias current of the junction increases. The energy spacing between the ground state and the first excited state is in the microwave range. The tunneling rate of the particle from the n^{th} energy level can be calculated by using the WKB approximation and describe the tunneling effect in the system. The tunneling rate of the higher level is more than the lower level and the tunneling rate of the ground state is less than the first excited state about three orders of magnitude. The probability of finding the fictitious particle can be explained by the wave functions which can be determined from solving the eigenvalue of Schrödinger equation numerically. The energy eigenvalue is in good agreement with the quantization energy and the eigenvector is qualitatively similar to the harmonic oscillator's because of the shape of the potential. The transition rate between the ground state and the first

excited state can be calculated analytically by considering the two-level system with a perturbation of the microwave current. If the frequency of the microwave current is equivalent to the energy spacing, the qubit oscillates between the ground state and the first excited state. The transition rate is important for building a quantum gate. Finally, the decoherence time of the Josephson junction due to a current noise can be calculated by observing the decay of the Rabi's oscillation. The decoherence time depends on the amplitude of the noise current and the deviation of the energy spacing with the bias current. The calculation is good agreement with the experiment.

These results show that the Josephson junction phase qubit satisfies the DiVincenzo's criteria and is a good candidate for a quantum computer. First, the energy levels in a single junction are well characterization for representing qubit and the physical system can be scaled-up in numbers utilizing existing fabrication technology. Second, the initial state can be prepared by cooling the system to extremely low temperature about millikelvin (depending on the kind of superconductors). Third, the Rabi's oscillation between the two states can be observed by using the microwave current with the frequency equivalent to the energy spacing. The period of the oscillation or the gate time is in order of nanosecond. Fourth, the quantum gates are constructed by using pulses of microwave current to perform qubit operations. Finally, one want to reduce the current noise in the junction to obtain a long decoherence time. For the 1000 operations, one must reduce the noise current to the order of 10 pA.

In this thesis, I studied a single Josephson junction as a qubit that is a basic knowledge of quantum computation. For the future work, the two or more qubits will be studied by coupling the Josephson junctions with a capacitance. The interaction between the junctions involving the effect of the coupling is very interesting. The equation of motion for the coupled circuit gives a new Hamiltonian for studying the quantum mechanical properties.

REFERENCES

1. Hughes, R. A quantum information science and technology roadmap. http://quist.lanl.gov, 2002.

2. Ramos, R. C., Gubrud, M. A., Berkley, A. J., Anderson, J. R., Lobb, C. J., and Wellstood, F. C. Desigh for effective thermalization of junctions for quantum coherence. *IEEE Trans. Appl. Supr.* **11** (2001): 998-959.

3. Feynman, R. P. Simulating physics with computers. *International Journal of Theoretical Physics* **21** (1982): 467-488.

4. http://www.intel.com.

5. Shor, P. W. Algorlithms for quantum computation: Discrete logarithms and factoring. *in Proc. 35th Annual Symposium on the Foundation of Computer Science*, edited by S. Goldwasser (IEEE Computer Society Press, Los Alamitos, California, 1994): 124-134.

6. Odlyzko, A. M. *The future of integer factorization.* AT&T Bell Laboratories preprint, 1995.

7. Nielsen, M. A., and Chuang, I. L. *Quantum computation and quantum information.* Cambridge: Cambridge University Press, 2000.

8. Bardeen, J., Cooper, L. N., and Schrieffer, J. R. Theory of superconductivity. *Phys. Rev.* **108** (1957): 1175-1204.

9. Tinkham, M. *Introduction to superconductivity.* New York: McGraw Hill, 1996.

10. Buckel, W., and Kleiner, R. *Superconductivity.* Weinheim: WILEY-VCH, 2004.

11. Landau, L.D., and Lifshitz, E.M. *Statistical physics.* New York : Pergamon Press, 1980.

12. Stewart, W. C. Current-voltage characteristics of Josephson junction. *Appl. Phys. Lett.* **12** (1968): 277-280.

13. McCumber, D. E. Effect of ac impedance on dc voltage-current characteristics of superconductor weak-link junction. *J. Appl. Phys.* **39** (1968): 3113-3118.

14. Haviland, D., and Ågren, P. *Introduction to Josephson tunneling.* Nanostructure Physics, KTH, 2001.

15. Martinis, J. M., Devoret, M. H., and Clarke, J. Energy-level quantization in the zero-voltage state of a current-biased Josephson junction. *Phys. Rev. Lett* **55** (1985): 1543-1546.

16. Xu, H., Berkley, A. J., Gubrud, M. A., Ramos, R. C., Anderson, J. R., Lobb, C. J., and Wellstood, F. C. Analysis of energy level quantization and tunneling from the zero-voltage state of a current-biased Josephson junction. *IEEE Trans. Appl. Supr.* **13** (2003): 956-959.

17. Zettili, N. *Quantum mechanics concepts and applications.* Chichester: John Wiley & Sons Ltd., 2001.

18. Spiegel, M. R. *Mathematical handbook of formulas and tables.* Singapore: McGraw-Hill, 1968.

19. Gradshteyn, I. M., and Ryzhik, I. S. *Integrals, series and products.* New York: Academic, 1980.

20. Kopietz, P., and Chakravaty, S. Lifetime of metastable voltage states of superconducting tunnel junction. *Phys. Rev. B* **28** (1988): 97-110.

21. Landau, L.D., and Lifshitz, E.M. *Quantum mechanics : Non-relativistic theory.* New York : Pergamon Press, 1997.

22. Arfken. G. B., and Weber, H. J. *Mathematical methods for physicists.* San Diego: Harcourt/Academic Press, 2001.

23. Chow, K. S., Browne, D. A., and Ambegaokar, V. Quantum kinetics of a superconducting tunnel junction : Theory and comparison with experiment. *Phys. Rev. B* **37** (1988): 1624-1646.

24. Farrell III, W. J. *Quantum theory of the RF SQUID qubit.* University of Maryland College Park, Maryland, 2000.

25. Berkley, A. J., Xu, H., Gubrud, M. A., Ramos, R. C., Anderson, J. R., Lobb, C. J., and Wellstood, F. C. Decoherence in a Josephson junction qubit. *Phys. Rev. B* **68** (2003): 060502(4), Wellstood, F.C., private communication.

26. Faires, J. D., and Burden, R. *Numerical methods.* Pacific Grove, CA: Brooks/Cole Pub., 1998.

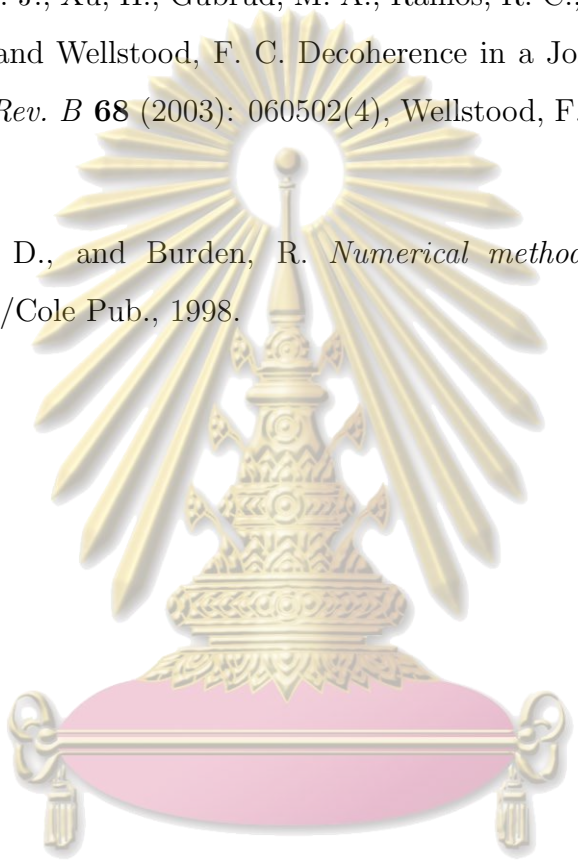

APPENDICES

APPENDIX A

CUBIC PARABOLA POTENTIAL

The cubic parabola potential can be approximated from the washboard potential,

$$U(\gamma) = -\frac{\hbar}{2e} I_c(\cos\gamma + \frac{I_{dc}}{I_c}\gamma). \tag{A.1}$$

The washboard potential is a series of the potential wells with the minimum points at $\gamma_0 = \sin^{-1} I'$, where $I_{dc}/I_c = I'$. When the bias current is close to the critical current ($I_{dc} \to I_c$) we can approximate this potential for considering only a potential well by changing the variable $\gamma \to q(\gamma)$ where $q(\gamma) = \gamma - \sin^{-1} I'$. The potential is rewritten as

$$\begin{aligned} U(q) &= -\frac{\hbar}{2e} I_c\{\cos(q + \sin^{-1} I') + I'(q + \sin^{-1} I')\} \\ &= -\frac{\hbar}{2e} I_c\{(1 - I'^2)^{1/2}\cos q - I'\sin q + I'(q + \sin^{-1} I')\}. \end{aligned} \tag{A.2}$$

The extremum points of the potential can be found by the condition $U'(q_0) = 0$,

$$\begin{aligned} (1 - I'^2)^{1/2}\sin q_0 + I'\cos q_0 - I' &= 0 \qquad (A.3) \\ \sin q_0 &= \frac{I'}{(1 - I'^2)^{1/2}}(1 - \cos q_0) \\ 2\sin\frac{q_0}{2}\cos\frac{q_0}{2} &= \frac{I'}{(1 - I'^2)^{1/2}}(2\sin^2\frac{q_0}{2}) \\ \tan\frac{q_0}{2} &= \frac{(1 - I'^2)^{1/2}}{I'} \\ q_0 &= 2\arctan\frac{(1 - I'^2)^{1/2}}{I'}. \qquad (A.4) \end{aligned}$$

From Eq.(A.3), the minimum point is $q_0 = 0$ and the maximum point is in Eq.(A.4). By using the approximation, $\cos q \approx 1 - q^2/2$ and $\sin q \approx q - q^3/6$,

the potential is rewritten as

$$U(q) = -\frac{\hbar}{2e} I_c \{(1-I'^2)^{1/2} + I' \sin^{-1} I' - (1-I'^2)^{1/2} \frac{q^2}{2} + I' \frac{q^3}{6}\}. \quad \text{(A.5)}$$

At the maximum point, q_0 can be approximated by $2\arctan(1-I'^2)^{1/2}/I' \approx 2(1-I'^2)^{1/2}/I'$ when $I' \to 1$. The barrier height of the potential can be calculated by

$$\begin{aligned} U_0 &= U(q_0 = 2\frac{(1-I'^2)^{1/2}}{I'}) - U(q_0 = 0) & \text{(A.6)} \\ &= \frac{\hbar}{2e} I_c \frac{2}{3} \frac{(1-I'^2)^{3/2}}{I'^2}. & \text{(A.7)} \end{aligned}$$

The potential parameters q_0 and U_0 are given in terms of the critical current and the ratio of the bias current and the critical current. From Eq.(A.5), the potential with the reference at the minimum point ($q_0 = 0$) can be written as

$$\begin{aligned} U(q) &= \frac{\hbar}{2e} I_c \{(1-I'^2)^{1/2} \frac{q^2}{2} - I' \frac{q^3}{6}\} \\ &= \frac{\hbar}{2e} I_c \frac{2(1-I'^2)^{3/2}}{I'^2} \{(\frac{q}{q_0})^2 - \frac{2}{3}(\frac{q}{q_0})^3\} \\ &= 3U_0 (\frac{q}{q_0})^2 (1 - \frac{2}{3}\frac{q}{q_0}). & \text{(A.8)} \end{aligned}$$

This potential is known as the cubic parabola potential for representing the washboard potential when the bias current is close to the critical current ($I_{dc} \to I_c$).

APPENDIX B

THE MIDPOINT METHOD

The midpoint method is one of the 2^{nd} order Runge-Kutta methods for solving an ordinary differential equation numerically. Considering an initial value problem

$$\frac{dx}{dt} = f(t,x,y) \tag{B.1}$$

$$\frac{dy}{dt} = g(t,x,y) \tag{B.2}$$

with the initial conditions $x(t_0) = \alpha$ and $y(t_0) = \beta$ over an interval $a \leq t \leq b$, the numerical solutions of the differential equations can be estimated by

$$dx = f(t,x,y)dt \tag{B.3}$$

$$dy = g(t,x,y)dt \tag{B.4}$$

$$x_{i+1} = x_i + h[f(t_i + \frac{h}{2}, x_i + \frac{h}{2}f(t_i,x_i,y_i), y_i + \frac{h}{2}g(t_i,x_i,y_i))] \tag{B.5}$$

$$y_{i+1} = y_i + h[g(t_i + \frac{h}{2}, x_i + \frac{h}{2}f(t_i,x_i,y_i), y_i + \frac{h}{2}g(t_i,x_i,y_i))] \tag{B.6}$$

where $x_0, x_1, ..., x_N$ and $y_0, y_1, ..., y_N$ are the approximations of $x(t)$ and $y(t)$ at any step time, respectively under the step size $h = ((b-a)/N)$. The local error of this method is in $O(h^3)$, and the global error is in $O(h^2)$[26]. The numerical solutions of $x(t)$ and $y(t)$ can be calculated from Eq.(B.5) and Eq.(B.6).

APPENDIX C

THE HYPERGEOMETRIC FUNCTION

The hypergeometric functions are solutions of the hypergeometric differential equation

$$z(1-z)y'' + [c-(a+b+1)z]y' - aby = 0 \ , \tag{C.1}$$

which has a regular point at the origin. The hypergeometric function can be derived by using the Frobenius method to reduce the differential equation to

$$\sum_{n=0}^{\infty}(n+1)(n+c)A_{n+1} - [n^2+(a+b)n+ab]A_n z^n = 0 \ , \tag{C.2}$$

giving the indicial equation

$$A_{n+1} = \frac{(n+a)(n+b)}{(n+1)(n+c)}A_n \ . \tag{C.3}$$

Inserting the relation into the ansatz series

$$y = \sum_{n=0}^{\infty} A_n z^n \tag{C.4}$$

then gives the solution

$$y = A_0[1 + \frac{ab}{1!c}z + \frac{a(a+1)b(b+1)}{2!c(c+1)}z^2 + ...] \ . \tag{C.5}$$

This is called the regular solution, defined by

$$\begin{aligned} {}_2F_1(a,b;c;z) &= 1 + \frac{ab}{1!c}z + \frac{a(a+1)b(b+1)}{2!c(c+1)}z^2 + ... & \text{(C.6)} \\ &= \sum_{n=0}^{\infty}\frac{(a)_n(b)_n}{(c)_n}\frac{z^n}{n!} \ , & \text{(C.7)} \end{aligned}$$

where $(a)_n$ are Pochhammer symbols. The hypergeometric series is convergent for arbitrary a, b, and c for real $-1 < z < 1$, and for $z = \pm 1$ if $c > a + b$.

VITAE

Rachsak Sakdanuphab was born in November 2, 1981 in Prachubkirikhan province. He received his bachelor degree of science (first class honor) in physics from Kasetsart University in 2002. He was supported the financial by the Development and Promotion of Science and Technology Talents Project (DPST) during his study.

CONFERENCE PRESENTATION:

2005 R. Sakdanuphab and S. Chatraphorn. Quantum computation and A Josephson junction qubit. 13^{th} Science Seminar 2005, Faculty of Science, Chulalongkorn University (16-17 March; 2005).

2005 R. Sakdanuphab and S. Chatraphorn. Decoherence in Josephson junction phase qubit. 31^{th} Congress on Science and Technology of Thailand, Suranaree University (18-20 October; 2005).